Doctoral Dissertations   Graduate School

Summer 2004

Modeling of solid layer growth at a constant speed in a binary melt crystallization process

Zongwen Feng

Follow this and additional works at: https://digitalcommons.latech.edu/dissertations

MODELING OF SOLID LAYER GROWTH AT A CONSTANT SPEED

IN A BINARY MELT CRYSTALLIZATION PROCESS

by

Zongwen Feng, B.S.

A Dissertation Presented in Partial Fulfillment
of the Requirements for the Degree
Doctor of Philosophy

COLLEGE OF ENGINEERING AND SCIENCE
LOUISIANA TECH UNIVERSITY

May 2004

UMI Number: 3126169

INFORMATION TO USERS

The quality of this reproduction is dependent upon the quality of the copy submitted. Broken or indistinct print, colored or poor quality illustrations and photographs, print bleed-through, substandard margins, and improper alignment can adversely affect reproduction.

In the unlikely event that the author did not send a complete manuscript and there are missing pages, these will be noted. Also, if unauthorized copyright material had to be removed, a note will indicate the deletion.

UMI®

UMI Microform 3126169

Copyright 2004 by ProQuest Information and Learning Company.

All rights reserved. This microform edition is protected against unauthorized copying under Title 17, United States Code.

ProQuest Information and Learning Company
300 North Zeeb Road
P.O. Box 1346
Ann Arbor, MI 48106-1346

LOUISIANA TECH UNIVERSITY

THE GRADUATE SCHOOL

04/27/2004
Date

We hereby recommend that the dissertation prepared under our supervision

by___Zongwen Feng_____

entitled _Modeling of Solid Layer Growth at a Constant Speed in a Binary Melt_

___Crystallization Process_____

be accepted in partial fulfillment of the requirements for the Degree of

___Doctor of Philosophy_____

Supervisor of Dissertation Research

Head of Department

Department

Recommendation concurred in:

Advisory Committee

Approved:

Director of Graduate Studies

Dean of the College

Approved:

Dean of the Graduate School

GS Form 13
(5/03)

ABSTRACT

Melt crystallization is an attractive separation method for the purification of organics at a large scale. Because the geometry of the rigid crystal lattice is peculiar to the particular substance, most crystallization processes form eutectic systems. The kinetics of crystallization limit the rate in which crystal growth can occur without the incorporation of undesired impurity. If the rate of heat transfer exceeds the mass transfer rate of the impurity, the impurity can solidify, contaminating the product. In practice, one would like to specify a crystallization rate and determine the temperature profile of the crystallizer wall that would achieve this rate.

In this dissertation we combine analytic and numerical methods for predicting solid-layer growth from melt crystallization. First, we predict the wall temperature profile over time for achieving solid separation from the melt at a constant rate. Second, we predict the rate of crystallization (or solid formation) when the wall temperature is held constant at a certain value equal to the lowest temperature that is operationally feasible. Third, we predict the temperature distribution in each of the solid and liquid phases. By considering a temperature distribution in the solid phase and holding the liquid phase's temperature constant in the radial direction, an analytic model was developed by using dimensional analysis. This model was then extended numerically to account for a temperature distribution in each of the phases, liquid and solid. Applications of the two models were demonstrated with an example involving crystallization of para-

dichlorobenzene from the ortho-dichlorobenzene and para-dichlorobenzene binary melt. Results from both models were analyzed and compared.

Results showed that a lower initial concentration required a higher cooling rate of the crystallizer wall in order to maintain the same crystallization rate. Hence, less time was needed to reach the wall temperature operation constraint, thus leading to less solid layer growth. By comparing the results of the two models, one can conclude that the numeric model is preferred, since more crystal growth will occur under the same conditions as for the analytic model.

APPROVAL FOR SCHOLARLY DISSEMINATION

The author grants to the Prescott Memorial Library of Louisiana Tech University the right to reproduce, by appropriate methods, upon request, any or all portions of this Dissertation. It is understood that "proper request" consists of the agreement, on the part of the requesting party, that said reproduction is for his personal use and that subsequent reproduction will not occur without written approval of the author of this Dissertation. Further, any portions of the Dissertation used in books, papers, and other works must be appropriately referenced to this Dissertation.

Finally, the author of this Dissertation reserves the right to publish freely, in the literature, at any time, any or all portions of this Dissertation.

Author _____

Date _____5/8/'04_____

TABLE OF CONTENTS

vi

LIST OF TABLES

x

LIST OF FIGURES

xi

NOMENCLATURE

C constant

C_p, C_{pl} specific heat of liquid

f, F functions

h_l heat convection coefficient

j grid index

k_l thermal conductivity of liquid

k_s thermal conductivity of solid

L latent heat per unit volume of solid

M number of steps for Runge-Kutta method

n time level

N number of grid points in liquid phase

r radius

r_0 radius of crystallizer

R gas constant

s width of solid layer

s^c solid layer width when the wall temperature reaches the operation limit

t time

t^c the time at which the wall temperature reaches the operation limit

T_0 crystallizer wall temperature

T_0^c operation limit temperature

T_A^f liquidus temperature

T_b melt bulk temperature

T_{eu} eutectic temperature

T_l liquid phase temperature

T_m solid-liquid interface temperature

T_s solid phase temperature

u speed of solid layer growth

X_E mole fraction at eutectic point

X_{init} initial mole fraction in binary melt compound

X_{liquid} mole fraction in liquid phase

X_s mole fraction in solid phase

α, α_s thermal diffusivity of solid

α_l thermal diffusivity of liquid

η a variable defined as $r/\sqrt{4\alpha t}$

ε threshold of crystal growth rate

θ distribution factor for implicit scheme

ρ solid density

ρ_l liquid density

λ latent heat of crystallization

λ' sum of latent heat and sensible heat of the crystallization mass

ΔH_A^f molar heat of solidification

Δr space increment

Δs solid layer growth increment

Δt time increment

ACKNOWLEDGEMENTS

First of all, I would like to thank my wife, Xingui, who always encouraged and supported me in my studies. I would like to express my greatest appreciation to my advisor Dr. Raja Nassar who provided me the opportunity to study at Louisiana Tech University and gave me countless help all through my dissertation. I would also like to thank Dr. Weizhong Dai who helped me with his great patience and excellent guidance in building the models in my dissertation.

I would like to thank Dr. James Palmer who gave me a lot of valuable advice. I also want to thank Dr. Ben Choi, as one of my committee members, who helped me throughout my research.

I want to thank all my friends who helped me during my study.

Finally, I want to express my appreciation to Dr. Greechie for his help during my study at Louisiana Tech University.

CHAPTER ONE

INTRODUCTION

1.1 Introduction to Melt Crystallization

Melt crystallization for large-scale purification of organics has boomed over the past few years. In the USA alone, total on-stream capacity is at least one billion pounds per year[1]. There are two main factors that brought this growth. First are the escalating requirements for purification. Melt crystallization is a very effective unit operation to produce organic compounds at high purity grade (>99.99%)[2], and it can easily reach the ppm purity levels associated with crystalline materials. Second is the increasing environmental concerns. There is no organic solvent needed in the melt crystallization process; thus, there is no solvent emission and solvent recovery processes. Also, melt crystallization usually operates at relatively lower temperatures, which makes it more attractive because of low specific energy required[3, 4].

The technique is now routinely used to purify naphthalene, paraxylene, disubstituted benzenes, acrylic acid, monochloracetic acid, nisphenol A, and many other chemicals[1].

There are two main melt crystallization methods, directional crystallization and zone melting. Directional crystallization has been applied fairly extensively to the purification of both organic and inorganic chemicals, as well as metals. Most work has

1

been carried out by lowering cylindrical glass containers from hotter to cooler environments. Attempts have been made to enhance the efficiency of the method by stirring the melt internally or by rotation of the container. A rather different approach to enhanced efficiency has been followed by Anderson, who used centrifugal force during crystallization[79]. Other directional crystallization experiments have been designed primarily for the concentration and separation of trace impurities. Much work in directional crystallization has been devoted to studying the crystallization process itself, especially as it relates to characterizing phase diagrams, since it connects solidus and liquidus compositions. A more exotic, but nonetheless interesting application, is the measurement of thermal conductivities[80]. Directional crystallization has been carried out on milligram to multikilogram scale. While most directional crystallization has been carried out in the batch mode, a device has been described in which aluminum ingots were fed to a crystallizer from which a purified ingot emerged continuously.

Most chemical zone melting is carried out vertically, in cylindrical glass tubes. However, sporadic reports of advantageous use of horizontal or nearly horizontal refiners have appeared. In general, molten zones are moved downward from a free surface into the ingot being processed. Containers of other shapes and materials have been used. Zone melting has been carried out on milligram and even microgram charges[81]. A number of attempts have been made to apply zone melting to multikilogram charges of chemicals[82]. Continuous zone melting has been described in [83, 84]. Vertical zone melting is usually carried out at 10^{-4} to 10^{-3} cm·s^{-1}; speeds up to 3×10^{-2} cm·s^{-1} have been used without loss of effectiveness in systems having effective mixing of the liquid zones.

As zone-melting techniques have evolved, specialized procedures have been introduced in response to particular requirements. In an attempt to improve the efficiency of impurity rejection at the solidifying interface, a number of workers have sought to use centrifugal solidification as a means for enhancing matter transport [79].

Column crystallization has been used as one of the purification procedures in which slurry of crystals and melt is subjected to countercurrent contact. In one system, for example, the charge of material to be purified is contained in an annular, cylindrical chamber which also houses a metal helix. Rotation of the helix drives the crystals in one direction, while melt moves countercurrently. Under an applied temperature gradient, a concentration gradient results. Thus, the opposite ends of the column will contain material that is more (less) pure than the original. Continuous operation is relatively easily achieved by introducing feed at a central point and removing product and waste from the ends of the column.

1.2 Comparison with Other Separation Methods

1.2.1 Melt Crystallization Compared
with Solution Crystallization

Solution crystallization is best known for separating a pure solute from impure solutions. An example is crystallization of common salt from brine. Water is a cheap and harmless solvent and allows the process to run at a benign temperature. But when crystallizing nonpolar organics, solvent crystallization requires organic solvents which are typically neither cheap nor harmless. On a laboratory scale, their use is manageable; however, large-scale processing becomes expensive because of the effort expended in preventing solvent emissions.

One fact is that most organics have melting points that present quite practical processing temperatures without the addition of a solvent. Fig. 1.1 shows a compilation by Matsuoka, et al.[5] of the melting points of organics from the 1984 CRC handbook. Over 70% of these substances have melting points between zero and 200°C. These chemicals are prime candidates for melt crystallization.
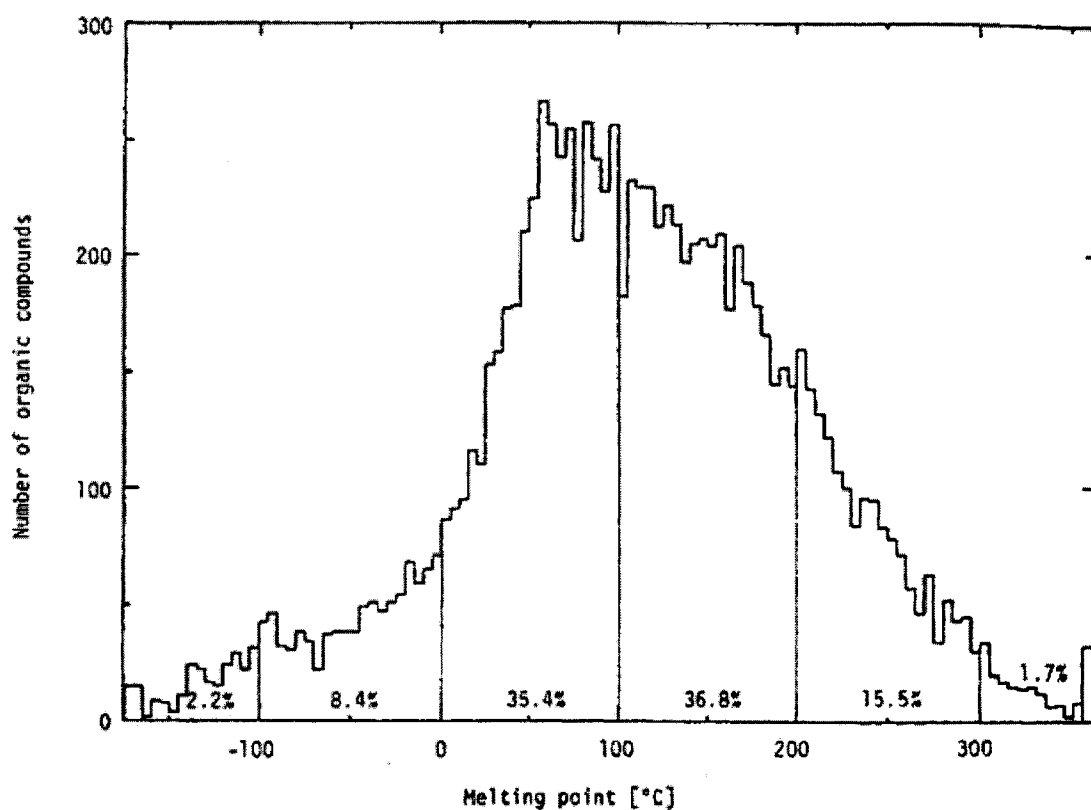
Fig. 1.1 Melting points of CRC organics [1]

Crystallization without using a solvent has a lot of advantages. The volume of material being processed is considerably less. Equipment costs and energy consumption are thus much lower. Further more, no solvent recovery is necessary. The impurities are recovered in molten form and can be recycled, incinerated, or treated in some other fashion, without an intermediate solvent-removal step. Also, the product is not

contaminated with solvent. Table 1.1 summarizes the key differences between melt and solution crystallization.

Table 1.1. Differences between melt crystallization
and solution crystallization

Melt Crystallization	Solution Crystallization
Compact equipment	Larger equipment
No solvent emissions	Potential for solvent emissions
No solvent recovery	Solvent recovery required
Higher operating temperatures	Lower operating temperatures
Higher viscosity fluid	Lower viscosity fluid
Moderate crystal growth rates	Higher crystal growth rates
Good selectivity	Better selectivity
Crystallization only by cooling	Evaporative crystallization possible

1.2.2 Melt Crystallization Compared with Distillation

Melt crystallization is superficially analogous to distillation since it uses solid-liquid equilibria to affect a separation, and distillation uses liquid-vapor equilibria. Both separation techniques depend on three elements:

- Phase equilibria which provide the driving force for separation

- Mass-transfer rates which allow phases to equilibrate

- Phase separability

However, the solid-liquid systems differ from vapor-liquid systems significantly in these critical areas. Table 1.2 shows the differences in the three aspects.

Table 1.2. Comparison of solid-liquid and vapor-liquid systems in separations

Melt crystallization(solid/liquid)	Distillation(vapor/liquid)
Phase equilibria	
Liquid phases are totally miscible; solid phases are not miscible	Both liquid and vapor phases are totally miscible
Typically, an eutectic system	Conventional vapor/liquid equilibrium
Solid phase is pure, except at eutectic point	Neither phase is pure
Partition coefficients are very high (theoretically, they can be infinite)	Separation factors are moderate and decrease as purity increases
Ultrahigh purity easy to achieve	Ultrahigh purity difficult to achieve
Recovery limited by eutectic compositions	No theoretical limit on recovery
Mass-transfer kinetics	
Only moderate mass-transfer rates in liquid phases, zero in solid	High mass-transfer rates in both liquid and vapor phases
Slow approach to equilibrium, included impurities cannot diffuse out of solid	Close approach to equilibrium achieved in brief contact time
Solid phase must be remelted and refrozen to allow phase equilibrium	Adiabatic contact ensures phase equilibrium
Phase separation	
Phase densities differ by only about 10%	Phase densities differ by a factor of 100 to 10,000
Liquid viscosity moderate, solid phase rigid	Viscosity in both phases low
Phase separation is slow; surface-tension	Phase separation is rapid and complete

effects prevent completion	
Countercurrent contacting is slow and imperfect	Countercurrent contacting is quick and efficient

From the table, we can see that equilibria are generally much more favorable in melt crystallization. Mass-transfer rates are much slower, however, so long residence times are needed for the bulk of the phases to approach equilibrium. This requires large equipment and makes the processing step costly. Also, phase separation after contacting – a trivial step for vapor-liquid systems – presents a problem for solid-liquid systems. Even with long residence times, complete separation is rarely achieved.

Lower temperatures pertaining to melt crystallization slow down the rate processes and make them critical. On the one hand, this is a drawback. However, it also highlights a situation in which melt crystallization finds its niche. If a material is prone to decomposition at distillation temperatures, it will likely be stable at its freezing point. Compared with distillation, melt crystallization may be slower, but it is also advantageous.

1.3 Application of Melt Crystallization to Organic Separations

A simple way of presenting where melt crystallization can be used to an advantage in organic separations is shown in Fig. 1.2. For mixtures of high relative volatility and whose components are thermally stable, distillation is normally the preferred separation technique. When relative volatility is low, distillation becomes more difficult and melt crystallization is likely to be more attractive. If thermal stability is very low, then solution crystallization may be the only practical separation method.
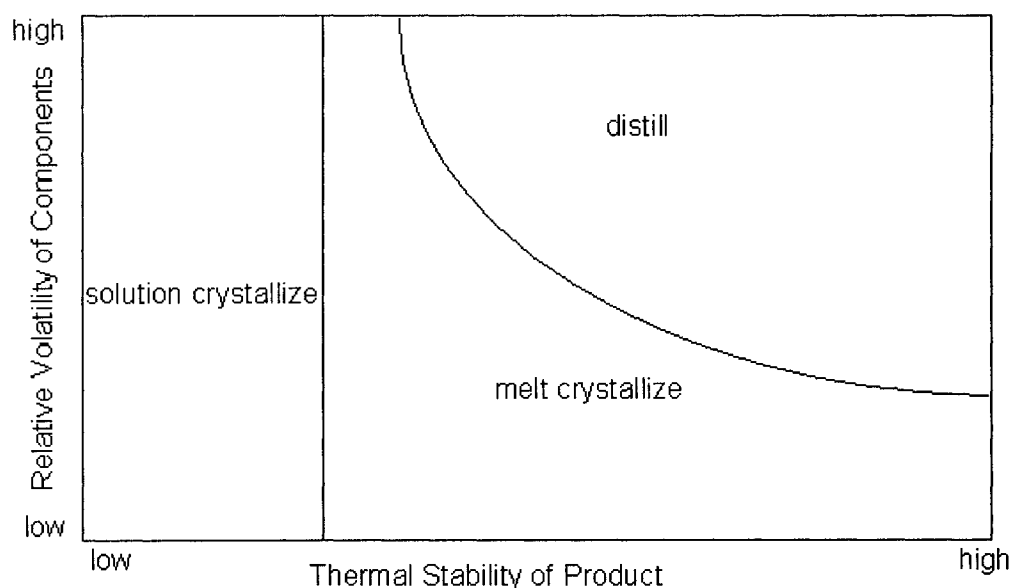
Fig 1.2. Applications of melt crystallization in organic separations

There are two types of melt crystallization systems: eutectic systems and solid-solution systems. The simple binary eutectic systems are mostly adapted during separation, and the eutectic systems with more than two components typically behave similarly to binary systems as long as the components do not interact with each other. A comparison of an eutectic system and a solid-solution system will be given in chapter two. The models built in this dissertation will only focus on simple binary eutectic systems.

1.4 Inverse Heat Conduction Problem

The Inverse Heat Conduction Problem (IHCP) is a problem of estimating the surface conditions such as temperature and heat flux, or surface properties such as thermal conductivity and heat capacity of solids by utilizing the transient temperature measurements taken within the medium[6-8]. IHCP is encountered in various branches of science and engineering. Mechanical, aerospace and chemical engineers, mathematicians,

astrophysicists, geophysicists, statisticians, and specialists of many other disciplines are all interested in inverse problems, each with different applications in mind. IHCP is of great importance because direct methods cannot be adopted in many cases. For example, direct measurement of heat flux at the surface of a wall subjected to fire at the outer surface of a reentry vehicle, or at the inside surface of a combustion chamber is extremely difficult. In such situations, the inverse method of analysis, using transient temperature measurements taken within the medium, can be applied for the estimation of such quantities.

IHCP is difficult to solve because it is an ill-posed problem[9-12]; that is, its solution does not satisfy the general requirement of existence, uniqueness, and stability under small changes to the input data. A variety of analytic and numerical approaches have been proposed for the solution of IHCP. Stoltz[13] was one of the earliest investigators who developed an analytic solution for a linear inverse heat conduction problem by using Duhamel's method, but the solution was found to be unstable for small time steps. This shortcoming was amended[14-16] through the use of future data concept; as a result, the improved solution permitted the use of much smaller time steps than that used in [13].

The analytic solutions developed by using integral or Laplace transform techniques[17-19] required continuously differentiable data; as a result, they were not so useful for practical applications; however, they provided a good insight into the nature of IHCP.

In order to cast IHCP as a well-posed problem, the traditional heat conduction equation was replaced by a hyperbolic heat conduction equation, and the well established techniques were used to solve the resulting IHCP[20].

The analytic solutions are strictly applicable to linear problems. To extend the technique to nonlinear problems, the numerical methods such as FDM [19, 21-28] and FEM[29-31] have been used in the solution of IHCP.

1.5 Research Objectives

Melt crystallization has become an attractive separation method to purify organics at large scale. Because the geometry of the rigid crystal lattice is peculiar to the particular substance, most crystallization processes form eutectic systems. The kinetics of crystallization limit the rate in which crystal growth can occur without incorporation of undesired impurity. If the rate of heat transfer exceeds the mass transfer rate of the impurity, the impurity can solidify, contaminating the product.

The melt crystallization process involves the problem of heat conduction or diffusion with a moving boundary. There are many mathematical models and numerical methods describing the inward solidification of a binary melt[32-61]. Among these, Chianese and Santilli[2] proposed an integral formulation approach to predict the growth of a crystal on a cylindrical cold surface in contact with a stirred melt. In their method, the trend of increase in solid-layer thickness is determined by an energy-integrated equation in which the temperature profile within the solid layer is approximated either using a second-degree polynomial or solving a steady-state heat transfer equation. Feltham and Garside[35] considered the solidification (freezing) of binary melts which are undercooled, and this means that the temperature of the melt lies below its equilibrium

freezing temperature, in which one of the components is preferentially rejected from the forming solid phase. They presented analytic and numerical solutions describing the inward solidification of a binary melt on a finite slab and sphere, respectively. The surfaces from which solidification commences were held at a constant temperature throughout the solidification process. Guardani, et al.[39] presented experimental results and simulation of static and dynamic solid-layer melt crystallization. The experiments were carried out in a static-layer crystallization, in which only natural convection influences mass and heat transfer, and in dynamic-layer crystallization, in which forced convection is obtained by pumping the mother liquor as a falling film on a heat exchanger. The solutions to the governing equation for the solid-layer thickness and temperature profiles over time were obtained by using an approximate analytic method. Nigro, et al.[47] considered the solid finite problem where the governing equations combine incompressible Navier–Stokes equations coupled with heat and mass transfer including phase change. A phase-wise discontinuous numerical integration of the finite-element method was presented to solve thermal phase-change problems in solidification processes. However, all of the present models and solutions consider that the surfaces from which solidification commences are held either at a constant temperature or at a constant convection on the surface where the solidification commences throughout the solidification process. A more useful approach is to specify a constant solidification speed and then determine the required surface cooling temperature in order to maintain an optimum crystallization cycle time. This is particularly important during the initial stages of crystallization, where heat transfer rates can exceed the mass transfer rates of the impurity, incorporating impurity into the solid product[62].

This separation process leads to an interesting inverse heat conduction problem since the outer cooling temperature is unknown. The solution to a traditional IHCP is usually unstable and very sensitive to input data, which are the internal temperatures measured through embedded devices. The problem that this dissertation considers is an IHCP problem. During crystallization, the solidification speed is specified precisely and there is no need for measuring the internal temperatures, so the system input errors do not exit. This makes the solution stable.

After the cooling surface temperature reaches an operational constraint imposed by the cooling utilities, the system holds this constant temperature and the crystallization continues. The problem then changes to the direct heat conduction problem since the outer wall temperature is known.

In this study, we will build models for an inward directional crystallization process with a moving boundary in a long cylindrical container. Two cases are considered: constant and variable liquid phase temperature in the radial direction. In each case, one first specifies a constant solidification speed and builds a model, for this inverse heat conduction problem, to predict the wall cooling temperature over time, which is required for obtaining this constant speed. Then, after the cooling wall temperature reaches a certain operating threshold, another model for the direct heat conduction problem is considered.

A comparison of the two cases and suggestions for using the models are presented.

1.6 Organization of This Dissertation

This chapter presents the general ideas of melt crystallization and the research objectives of this dissertation. In Chapter 2, the technical issues of melt crystallization including eutectic system and heat transfer equations are explained. In Chapter 3, a model is presented where only the solid phase is considered. In this case, the radial temperature in the liquid phase is assumed to be constant. In Chapter 4, we extend the model to include both a solid phase and a liquid phase with no restrictions on the temperature distribution in either phase. Both models are then illustrated with examples in Chapters 5 and 6.

CHAPTER TWO

DIRECTIONAL CRYSTALLIZATION

Directional crystallization processes have been commercially operated for the separation and purification of a number of chemical products, and they are based on the growth of a solid layer adjacent to a cooled surface by freezing a melt under controlled conditions of heat exchange.

Directional crystallization may be carried out in three ways: cylindrical/axial, cylindrical/radial, and spherical/radial, as illustrated in Fig. 2.1.

In cylindrical/axial mode, a cylinder of liquid, at a temperature slightly above the crystallization temperature of the contents, is moved through a temperature gradient into a cold zone in such a way that the contents of the tube crystallizes (Fig. 2.1a). Because the solidifying interface is perpendicular to the axis of the container, this process has also been called "normal freezing." Another mode of generating a solid cylinder from a melt is to "pull" a crystal on a cooled rod from a vessel containing the melt. This tactic, long used for growth of single crystals, is known as the Czochralski method[64].

In cylindrical/radial mode, the solidification procedure may be carried out in one of two modes, namely, radially inward and radially outward (Fig. 2.1b). In the former, a cylindrical sample container is immersed in a thermostat bath whose temperature is slightly lower than the freezing temperature of the contents of the tube. This geometry

14

produces gradual inward solidification from the cylindrical wall at a rate that diminishes with time, as a result of the thermal impedance of the solid that is forming. In the latter, a cylindrical sample container is provided with a hollow axial tube through which coolant may be circulated in such a way that outward solidification will proceed on the inner tube toward the wall of the cylindrical container.

(a)   (b)   (c)
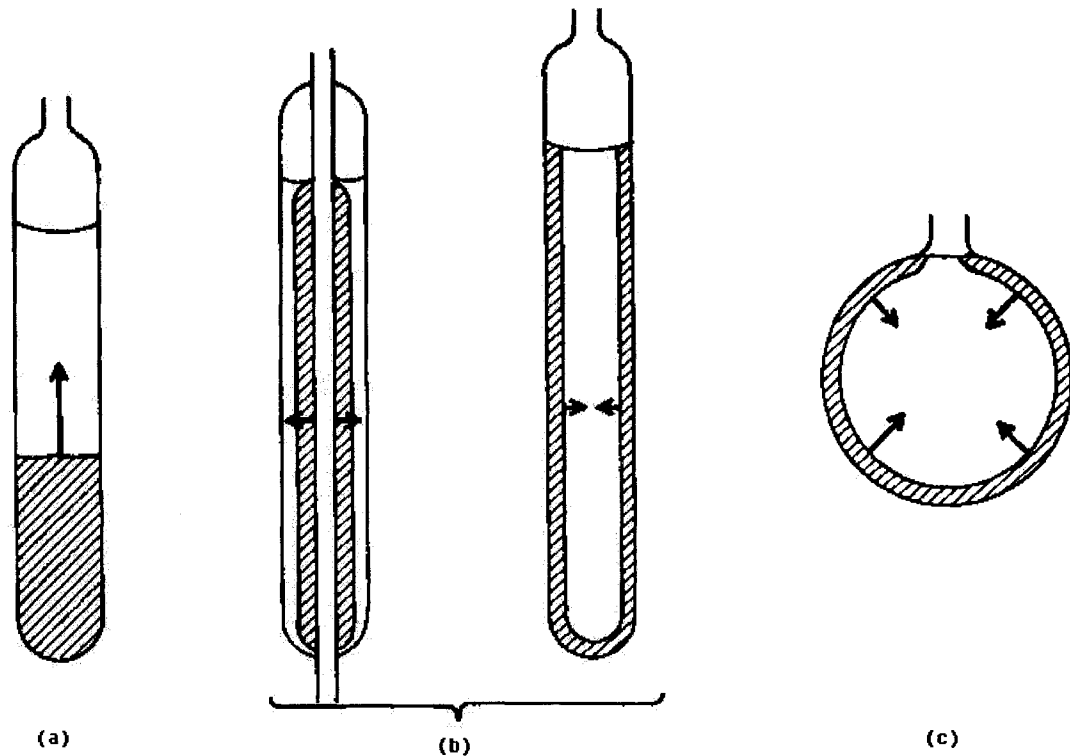
Fig 2.1 Modes of directional crystallization[64].
(a) cylindrical/axial; (b) cylindrical/radial; (c) spherical/radial.

In the spherical/radial mode, the sample is contained in a sphere, which may be a round-bottom flask; it is immersed in a cooling bath and a heat source is placed at its center. Radial solidification takes place inwardly, leaving a small fraction molten in the vicinity of the central heater (Fig. 2.1c).

All the processes are conceptually transient, since during the crystallization process the solid layer thickness increases continuously, causing continuous change in process conditions. The separation efficiency in layer crystallization processes is affected not only by the initial concentrations of the components, but also by the thermal properties of the components, the crystallization speed, as well as the dimensions of the crystallizer.

The crystallization technique is in essence very simple. If an impure molten material is cooled to its freezing point and more heat is removed, then some of the material will solidify. On the other hand, directional crystallization problems are moving boundary problems and there are phase changes with the moving solid-liquid interface; thus, it is difficult to achieve one direct solution. For a better understanding of the problem, this chapter introduces the phase rule and some heat transfer properties of the system.

2.1 Phase Rule

As one of the important separation methods for organics in industry, melt crystallization can be classified into two types of systems: those forming eutectics and those forming solid solutions. Most crystalline solids tend not to form solid solutions because the geometry of the rigid crystal lattice is peculiar to the particular substance. Impurities cannot fit in when these molecules are of a different size or shape. When a crystal is formed, such impurities will be rejected from the lattice. If the temperature is low enough that two components are solidified, then two distinct solid phases will be formed even though they may be intermixed on a macroscopic scale[1].

This situation can be explained further using the Phase Rule. The Phase Rule is simply stated as follows:

$$P + F = C + 2 \tag{2.1}$$

where P is the number of phases, F is the number of degrees of freedom, and C is the number of components. If pressure is held constant, the number of degrees of freedom is reduced by one and the Phase Rule becomes:

$$P + F = C + 1. \tag{2.2}$$

Consider, for example, a binary system where C takes a value of 2. The number of degrees of freedom can then be expressed as

$$F = 3 - P. \tag{2.3}$$

Different phases formed by a binary system can result in different degrees of freedom of the system. This is illustrated in Table 2.1.

Table 2.1 Relationships of phase and
degrees of freedom for a binary system

Phase (P)	Degrees of Freedom (F)
1	2
2	1
3	0

We consider a binary melt as one phase (liquid). If none of the solids exist, the phase number is 1, thus the system has two degrees of freedom. This means that the concentrations of the two components vary in the liquid state (the melt is not fully stirred). If the two components can only form two solid states of their own, the phase number becomes 3, then the system has zero degree of freedom (this is the eutectic

system introduced in the following section). If the binary melt can only form one solid state, the phase number is 2 and the system has a freedom of 1 (this is the solid solution system in section 2.1.2). The number of solid states that the compound melt can form depends on the molecular structures of the components. Different components may form different kinds of systems. When considering whether the solid states of two components are miscible or not, the phase equilibrium can be classified into two systems as follows.

2.1.1 Eutectic Systems

If two components are not miscible, there will be only two solid states for the two components. With the addition of the liquid phase of the two components, at most three phases can coexist with P=3. This means that only three phases can coexist at one single point (zero freedom) in a composition vs. temperature plot. The point at which the three phases coexist is called the eutectic point. At all other compositions, a liquid phase can coexist with only a single solid phase. However, in the absence of solid solutions, a single solid phase can consist of only one component. It follows that only pure solid can be in equilibrium with a liquid mixture, except at a single point on the phase diagram. Systems exhibiting such behavior are called eutectic systems.

2.1.1.1 Phase Diagram. The characteristic phase diagram for a simple binary eutectic system is shown in Fig. 2.2.

The freezing behavior of a two-component (A and B) mixture of initial composition X_i and temperature T_i is depicted in Fig. 2.2. When the mixture is first cooled, the temperature drops to T_F without any concentration or phase change. The mixture is now at its freezing point. Further cooling results in the formation of pure solid B, and progressive depletion of component B in the liquid shifts the liquid composition to

the left on the diagram. At the same time, the freezing point decreases through point L towards the eutectic point E. Note that before the eutectic point E is reached, only component B has been crystallized. When the temperature reaches T_E, then further cooling results in simultaneous crystallization of both A and B at a constant temperature. Only when all the material is frozen will the temperature fall below the eutectic temperature T_E. The line T_B-F-L-E-T_A is known as the liquidus line since the system contains only liquid in the area above this line.

Note that the composition of the liquid fraction follows the liquidus line as the mixture is cooled. The net composition of the total mixture stays constant, however, and at a temperature T_L, the mixture is represented by the point M. Used in this way, phase diagrams also give information on the relative amounts of solid and liquid in equilibrium. Since the mixture M consists of liquid of composition X_L and pure solid B, the lever rule can be used to calculate the amount of solid and liquid. The rule can be remembered by imagining W_L lbs of liquid and W_S lbs of solid placed at opposite ends of a lever L-M-S with its fulcrum at point M. To balance the lever,

$$W_L * LM = W_S * MS, \tag{2.4}$$

where LM and MS represent the lengths from point L to M and M to S, respectively. The actual shapes of the liquidus lines are normally determined experimentally. However, under certain simplified assumptions they can be represented by thermodynamic expressions.
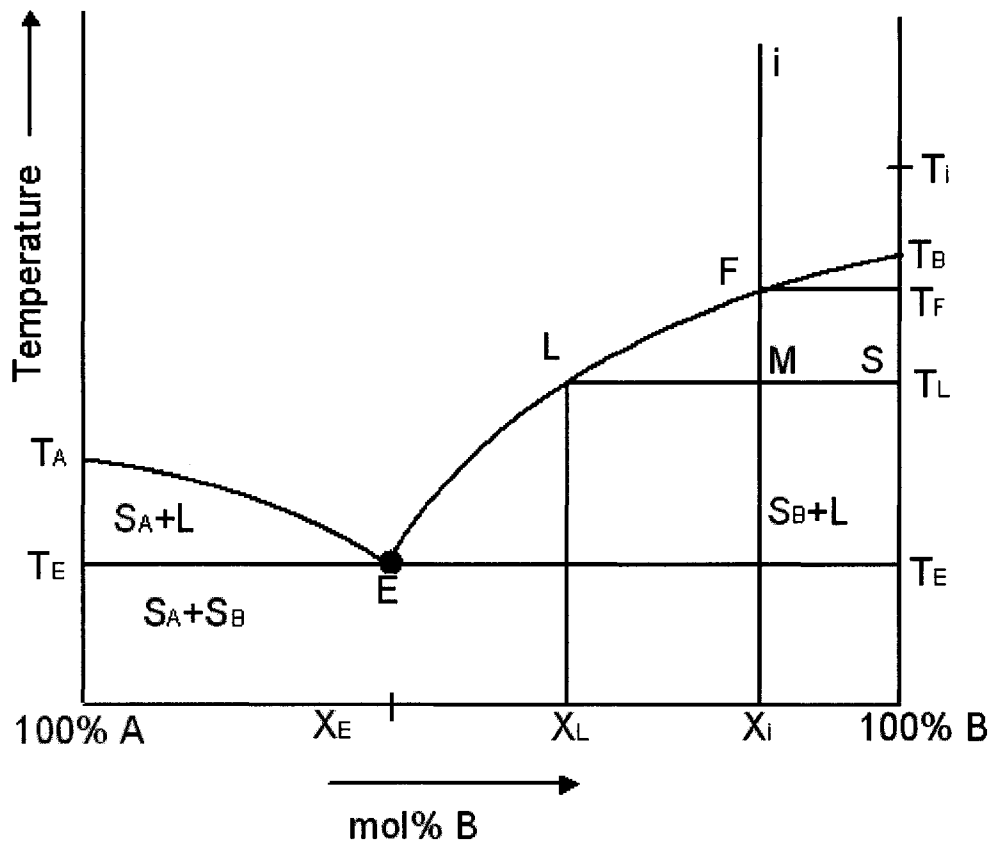
Fig. 2.2 Phase diagram for binary eutectic systems

2.1.1.2 Van Laar Equation. If A and B form perfect solutions and if the solid and liquid have equal heat capacities, then the liquidus line for component A is given by[1]

$$\ln X = \frac{\Delta H_{f,A}}{R(1/T - 1/T_A)}$$ (2.5)

where X is the mole fraction of component A in the mixture, $\Delta H_{f,A}$ is the molar heat of fusion of component A, R is the gas constant, T is the liquidus temperature, and T_A is the freezing point of pure A. Similarly, for component B, we have

$$\ln(1 - X) = \frac{\Delta H_{f,B}}{R(1/T - 1/T_B)}.$$ (2.6)

The eutectic point lies at the intersection of the two lines.

<u>2.1.1.3 Eutectic Temperature.</u> By setting $T_A = T_B = T_{eu}$, we can solve equations (2.5) and (2.6) to achieve the eutectic temperature, T_{eu}, which is the minimum temperature at which only one pure component can be solidified out. It is also the temperature where the melt phase is in equilibrium with two solid phases (i.e., the free energy curve of the melt and the free energy of two solid phases lie on the same common tangent). The composition of the melt phase at the eutectic temperature is referred to as the eutectic composition. A melt with a bulk composition equal to the eutectic composition will transform directly to an intergrowth of the two solid phases on cooling through the eutectic temperature (the eutectic reaction). Below the eutectic temperature, there is a broad two-phase field consisting of an intergrowth of the two solid phases. As such, the cooling constraint of solidification utilities should be set to be above this eutectic temperature.

2.1.2 Solid-Solution Systems

Solid-solution systems occur when impurity molecules are included in the crystal lattice. In organic systems, this occurs typically by substitution of host molecules rather than by inclusion in interstitial voids. Solid solutions occur in a minority of cases only since the guest molecule must be of a similar size and shape to the host molecule to minimize any distortion of the crystal lattice. A simple binary solid-solution case can be considered as a counterpart of the simple binary eutectic system discussed above. The example below is for a system where solid solubility is mutual and continuous, i.e., it occurs over the whole range of composition. As shown above, the phase rule for a binary system at a constant pressure reduces to

$$F = 3 - P \tag{2.7}$$

When considering mutual solid solubility, there can only be one solid phase, but it will typically consist of a mixed crystal, i.e., a crystal containing both A and B. If both liquid and solid are present, then

$$P = 2 \quad \text{and} \quad F = 1 \tag{2.8}$$

In this case, fixing the temperature defines the state of the system, i.e., the relative amounts of A and B in coexistent solid and liquid phases are specific functions of temperature only. Fig. 2.3 shows a phase diagram for this type of system. It takes the same form as the more familiar McCabe-Thiele vapor-liquid equilibrium, another case where only two phases can arise.

Consider, again, cooling and crystallizing a mixture at an initial temperature T_i and an initial composition X_i. Solidification starts at T_F with a solid phase of Y_F mol% of component B and $(1-Y_F)$ mol% of component A. As crystallization progresses, the concentration of B in the melt decreases. The composition of the melt shifts from X_F through X_H at T_H to X_J at T_J. At the same time, the crystal composition shifts from Y_F through Y_H to Y_J at T_J, and solidification is complete when $Y_J=X_i$. The lower line in this phase diagram indicates the temperature at which a solid mixture just starts to melt and is called the solidus line.
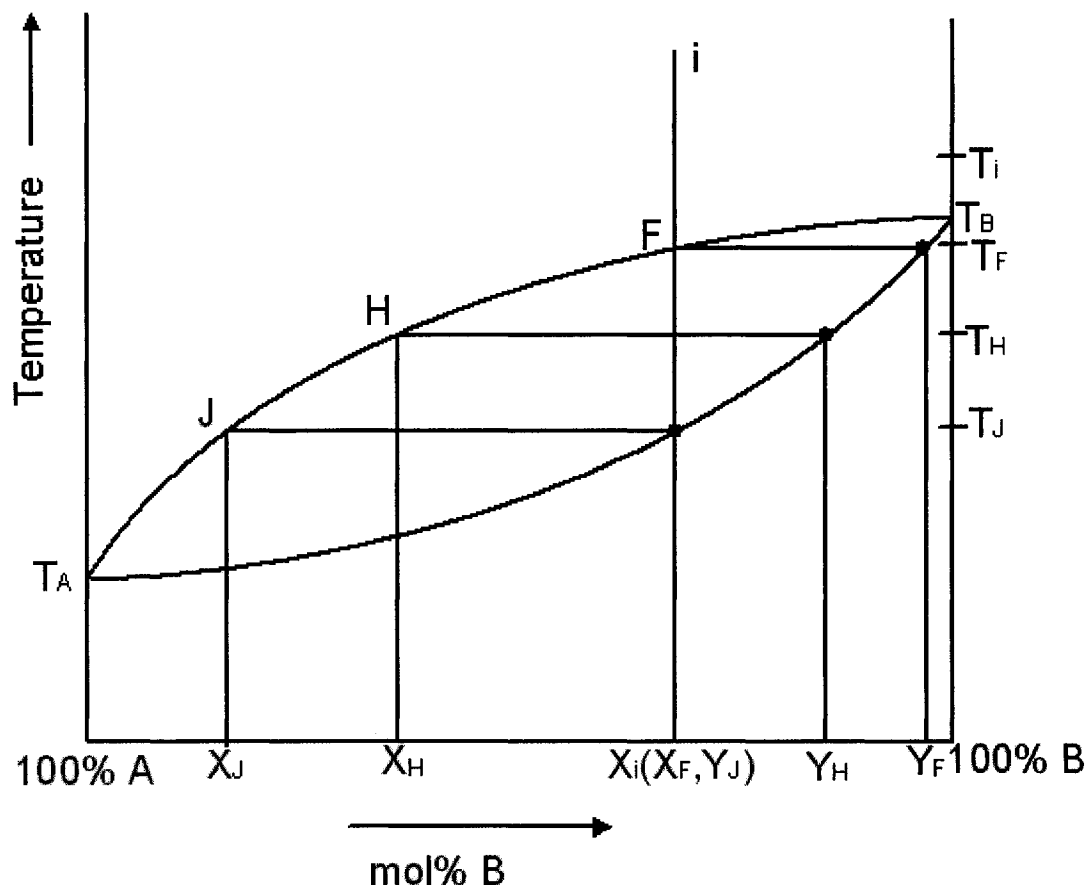
Fig. 2.3 Phase diagram for a binary system with continuous solid solubility

2.1.3 Complex Systems

Melt crystallization is often used to separate isomers after other impurities have been separated by distillation. These systems are typically binary or ternary eutectics. Systems with more than two components typically behave similarly to binary systems if the components do not interact with each other.

More complicated situations with eutectic systems can arise if one of the components exhibits polymorphism or if some of the components react to form other compounds. The existence of solid solutions further complicates the picture, since solid solubility is often limited to certain concentration ranges. Differing extents of solid

solubility can give rise to quite different phase diagrams. An excellent survey of this topic is available in [64].

Matsuoka[5] categorized all the organic mixtures in the ICT for which phase diagrams could be found. Over 50% exhibited simple binary eutectic behavior. Only 14% show partial or total solid solubility. This means that most organic mixtures can, in theory, be purified completely in a single stage of melt crystallization. The only restriction is that enough of the crystallizing component must remain liquid to prevent the liquid from approaching the eutectic composition. This, of course, limits the recovery, particularly if the starting material is of low purity.

2.1.4 Determination of Phase Diagram

Engineering design of crystallization systems requires knowledge of an entire phase diagram; eutectics, peritectics, and compound formation can exert decisive influence on the effectiveness of crystallization processes as industrial techniques. If there is a phase transformation near the solidus, it may affect the course of purification in that a volume change or a heat effect associated with such a transformation could result in entrapment of an impure melt at the interface.

There are four major techniques, which may be used for establishing the solidus and liquidus curves of binary systems: (1) thermal microscopy, (2) thermal analysis, (3) zone melting, and (4) single-crystal growth. These techniques are not all universally applicable, and some have only limited utility. The choice of method will depend on a number of factors. These include: availability of instrumentation, amount of material and time available, environment mental sensitivity of the components, and temperature range. Thermal microscopy and thermal analysis may be carried out with milligram or even

microgram quantities, while zone melting and single-crystal growth methods require gram quantities. However, thermal microscopy and thermal analysis require considerably more costly instrumentation than the other methods. It is fairly easy to carry out methods 3 and 4 in evacuated, sealed vessels. While the sample to be used in methods 1 and 2 may also be enclosed in a sealed container, the sample preparation must be carried out in a glovebox if it is necessary to exclude air completely from the sample. Naturally, method 1 could not be applied to a material or system that is photodegraded at or near its melting point.

It must be pointed out that the four methods above are by no means a complete compendium of techniques applicable to the determination of phase diagrams. Any physical property that changes discontinuously during a liquid/solid phase transition can, in principle, be used to obtain liquidus and solidus curves. Line widths in nuclear magnetic resonance spectra[85, 86, 87], exchanges in electrical resistivity, mechanical properties, X-ray diffraction, and electrochemical methods[88] have all been used. In recent years, powerful methods have emerged for recognizing the appearance of phases in very small samples. Other exotic methods have been reviewed by Rhines[89]. Table 2.2 summarizes the common methods for determination of phase diagrams.

Table 2.2 Summary of Experimental Methods
for Determination of Phase Diagrams[64]

Technique	Range, %	Amount Required	Speed	Accuracy	Equipment Cost, $M, 1986
Thermal Microscopy	0-100	mg or less	High	High	5-7

DTA/DSC	0-100	Tens of mg	High	Moderate	20-30
Cooling/heating Curves	0-100	1-10g	Low	Moderate	0.5-5
Zone refining	0-10	0.0-10g	Low	Moderate	1-5
Temperature gradient oven	0-10	1-10g	Low	High	2-10
X-ray diffraction	0-100	Mg	Low	Moderate	>10
Dilatometry	0-100	1-10g	Low	Moderate	1-2

2.2 Crystallization Rate

Crystals grow from melts at widely varying rates. Organic crystals typically grow at rates less than 3×10^{-4} cm/s, ionic crystals at about 10^{-3} cm/s, and metals at rates up to 10^{-1} cm/s[64]. The differences result from the differing activation energies required to move atoms, ions, or molecules from the melt to the crystal surface through the boundary layer around the crystal. The growth rates also depend on associated entropic changes. For small, symmetrical crystallizing unit (atoms), the activation energy is low. For large, unsymmetrical units (organic molecules), it is high.

The calculation of crystallization rates has been approached from both thermodynamic and statistical viewpoints. In the former, the rate is considered at the rate of nucleation and calculated from the free energies of solid, melt, and an activated state in the melt. The expression for nucleation rate is

$$\frac{dZ}{dt} = K \exp\left(-\frac{\Delta G^*}{kT}\right)\exp\left(\frac{\Delta G_A}{kT}\right) \tag{2.9}$$

where Z is the number of nuclei, ΔG_A is the activation energy for transfer of atoms from the melt to the crystal surface by diffusion, ΔG^* is the excess free energy of the critical cluster, t is time, T is temperature, and

$$K = nn' \frac{kT}{h} \tag{2.10}$$

where n is the number of atoms per unit volume in the system, n' is the number of atoms on the surface of the critical nucleus.

Eq. (2.9) predicts zero growth rate at $T=0K$ and $T=T_f$, with a maximum at some intermediate temperature, T_{max} (T_f is the equilibrium crystallization temperature of the melt).

2.3 Distribution Coefficient

Crystal is a regularly repeated array of a characteristic building block. The specific binding forces that lead to the regularity of the crystal lead to the exclusion of foreign molecules. If solidification takes place rapidly, then the local composition of the resulting solid will be very close to that of the original liquid. On the other hand, if solidification is slow, then the crystal architecture of the major component of the mixture may direct the chemical composition of the solid that forms. The selectivity of crystallization depends upon the specific intermolecular forces acting among the constituent molecules, and these forces are determined by the relative sizes, shapes, and polarities of the constituent molecules. Considering that the sizes of organics are regularly large, the driving forces for crystallization is weak. This results in the

requirement of relatively low solidification speed in order to purify one component. In most cases, the crystal formed is not 100% pure. The purification efficiency is described by distribution coefficient,

$$k = \frac{C_s}{C_l}$$
(2.11)

where C_s is the concentration of the minor component in the solid and C_l is the uniform concentration of the same component in the liquid, at the liquid/solid interface. The ideal distribution coefficient is 0 since $C_s = 0$ means there is no impurity in the crystal. When $k = 1$, then C_s is equal to C_l, and there is no purification at all.

2.4 Heat Transfer Coefficients

To better understand the problem, several parameters need to be explained.

2.4.1 Thermal Conductivity

Thermal conductivity (k) represents the effectiveness of a material as a thermal insulator. The energy transfer rate through a body is proportional to the temperature gradient across the body and its cross sectional area. The fundamental law of heat conduction is given as

$$Q = k \cdot A \cdot \frac{dT}{dx},$$
(2.12)

where Q is the heat flow (W), k is the thermal conductivity value (W/(m K)), A is the cross-sectional area (m^2), and dT/dx is the temperature/thickness gradient (K/m).

A substance with a large thermal conductivity value is a good conductor of heat, and one with a small thermal conductivity value is a poor heat conductor, i.e., a good insulator. Hence, knowledge of the thermal conductivity value allows quantitive

comparisons to be made between the thermal insulation efficiencies of different materials. The most effective insulation will have a very low thermal conductivity value.

2.4.2 Thermal Diffusivity

Thermal diffusivity (α) of a medium is the thermophysical property that determines the speed of heat propagation by conduction through the medium. The higher the thermal diffusivity, the faster the heat propagation. Thermal diffusivity is related to the thermal conductivity, density, and specific heat of the medium:

$$\alpha = \frac{k}{\rho \cdot c_p},$$ (2.13)

where α is thermal diffusivity (m^2/s), k is thermal conductivity (W/(m K)), ρ is density (g/m^3), and c_p is specific heat (J/(s K)). According to the above definition, thermal diffusivity affects any conductive transient heat transfer process within the medium.

2.4.3 Specific Heat

Specific heat (c_p) is the amount of energy needed to raise the temperature of one gram of a substance by 1°C. The relationship between heat and temperature change is usually expressed in the form shown below:

$$Q = c_p \cdot m \cdot \Delta T,$$ (2.14)

where Q is the heat added, c_p is the specific heat, m is the mass, and ΔT is the temperature change. This relationship does not apply if a phase change is encountered because the heat added or removed during a phase change does not change the temperature.

2.4.4 Latent Heat

Latent heat is encountered whenever a phase change occurs. Latent heat is the heat released or absorbed per unit mass by a system in a reversible isobaric-isothermal

change of phase. The heat will only change the structure or phase of the material, e.g. melting or boiling of pure materials. In meteorology, the latent heats of evaporation (or condensation), fusion (melting), and sublimation of a water substance are of importance. The driving force behind latent heat is called the first law of thermodynamics, more commonly known as conservation of energy. One can say energy is conserved in that it is not destroyed or created anew, but simply changes form. In a melt crystallization process, the solid-liquid interface moves and there is a phase change at the interface, causing latent heat to be generated along the interface. As such, any modeling of a moving boundary problem should consider latent heat as a critical factor.

2.4.5 Interface Equations

The regions occupied by the solid and liquid phases are linked by the conservation of heat flux at the interface. Theoretically, both liquid and solid phases have temperature distributions, and the governing equation at the interface is only related to the temperature profiles near the interface. For modeling purposes, we consider two situations, one where the melt or liquid temperature is constant in the radial direction and the other where the temperature varies.

2.4.5.1 Constant Melt Temperature in the Radial Direction. We can simplify the problem by considering the melt temperature to be constant. This is a feasible assumption in an experiment where the melt is fully stirred. This causes all positions in the melt to have the same temperature, T_b. As the solid layer grows, the bulk temperature will decrease with the interface temperature. The governing equation for this situation may be expressed as[2]

$$-k\left(\frac{\partial T_s}{\partial r}\right) = \rho\lambda' \frac{ds(t)}{dt} + h_l(T_b - T_m), \quad r = r_0 - s(t) \tag{2.15}$$

where k is the thermal conductivity of the solid layer, ρ is crystal density, and h_l is the heat convection coefficient. T_m is the interface (melting) temperature as determined by the Van Laar equation, T_b is the temperature of the melt bulk, and λ' represents the sum of the heat released by crystallization, λ, and of the sensible heat of the crystallized mass:

$$\lambda' = \lambda + C_p (T_b - T_m).$$ (2.16)

Here, C_p is the specific heat.

2.4.5.2 Variable Melt Temperature in the Radial Direction. When the liquid is held still, a temperature gradient is formed in the radial direction. The temperature decreases from the center of the cylinder crystallizer to the solid-liquid interface. In this case, the interface equation is given as[43]

$$-L\frac{ds(t)}{dt} = k_s\left(\frac{\partial T_s}{\partial r}\right) - k_l\left(\frac{\partial T_l}{\partial r}\right), \quad r = r_0 - s(t).$$ (2.17)

Here, L is the latent heat per unit volume of solid, k_s and k_l are the heat conductivity coefficients of the solid and liquid layer, respectively. This equation states that the difference in heat flux across the interface is equal to heat absorption or heat liberation at $r = r_0 - s(t)$.

CHAPTER THREE

MODELING OF BINARY MELT CRYSTALLIZATION

WITH A CONSTANT LIQUID TEMPERATURE

IN THE RADIAL DIRECTION

3.1 Introduction
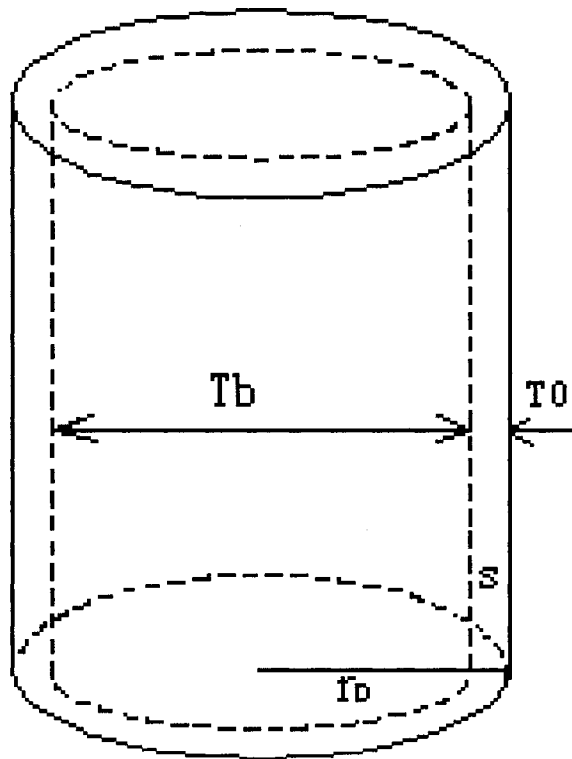
Figure 3.1 Schematic view of a three-dimensional solidification problem

32

This study deals with the modeling of melt crystallization through a temperature controlled cylindrical container as illustrated in Fig 3.1. The binary melt in the container is first preheated to a certain level higher than the eutectic temperature of the compound. Then, the melt is cooled down by cooling the wall of the container causing one component to solidify out and a solid layer to grow along the wall toward the center of the container.

In this model, we assume that the liquid is fully stirred, so the melt has a constant temperature during the process. We also assume that the solid remains pure and all the impurities remain in the liquid. This is a reasonable assumption for eutectic systems as long as the solidification speed does not exceed a certain threshold.

If the ratio of the length of the cylinder to its radius is large, one can simplify the model from three- to two-dimensions as shown in Fig 3.2.
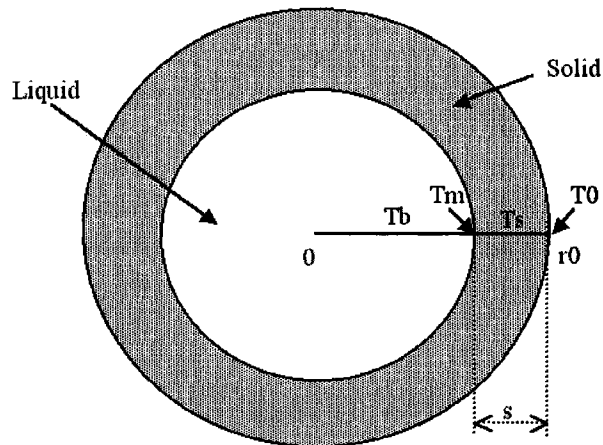
Figure 3.2 Simplified two-dimensional scheme

Since the two-dimensional problem in Fig 3.2 is circular, we can simplify the problem further to a one-dimensional case as illustrated in Fig. 3.3.
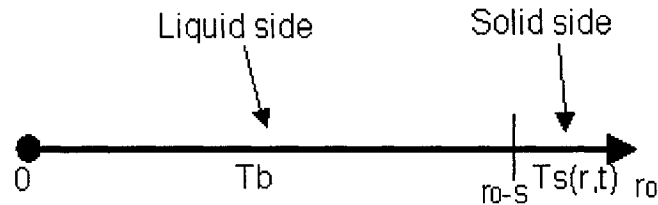
Figure 3.3 Simplified one-dimensional scheme

Finally, the one-dimensional case is solved to obtain the temperature distribution along the radius of the solid.

3.2 Solid Governing Equation

For the solid layer, the heat transfer equation is given as

$$\frac{1}{\alpha}\frac{\partial T_s}{\partial t} = \frac{1}{r}\frac{\partial}{\partial r}(r\frac{\partial T_s}{\partial r}), \quad r_0 - s(t) < r < r_0 ,$$ (3.1)

where T_s is the temperature in the solid side, α is the heat diffusivity within the solid phase, $s(t)$ is the solid layer thickness, and r_0 is the radius of the cylinder.

3.3 Solid-Liquid Interface Equation

The solid-liquid interfacial equation of the problem is described as follows:

$$-k_s\left(\frac{\partial T_s}{\partial r}\right) = \rho\lambda'\frac{ds(t)}{dt} + h_l(T_b - T_m), \quad r = r_0 - s(t) ,$$ (3.2)

where λ' represents the sum of the heat released by crystallization, λ, and of the sensible heat of the crystallized mass, and

$$\lambda' = \lambda + C_{pl}(T_b - T_m).$$ (3.3)

In Eqs. (3.2) & (3.3), T_b is the temperature of the melt bulk, T_s is the temperature of the solid crystal layer, ρ is the density, h_l is the heat convection coefficient, k_s is the heat

conductivity coefficient of the solid layer, C_{pl} is specific heat, and T_m is the melting temperature determined by the Van Laar equation[65, 66]

$$\ln(X_{liquid}) = \frac{\Delta H_A^f}{R}(\frac{1}{T_A^f} - \frac{1}{T_m}),$$ (3.4)

$$\text{where } X_{liquid} = \frac{r_0^2}{[r_0 - s(t)]^2}(X_{init} - X_S) + X_S$$ (3.5)

Here, X_{init} is the initial composition of the compound, and X_s is the composition of the solid that has been solidified out.

3.4 Boundary Conditions

For this problem, we assume that the wall temperature T_0 is set equal to the temperature of the solid at position $r=r_0$, and the interface temperature, which is also the melting point, is set equal to the temperature of the solid at $r=r_0-s(t)$. These conditions are described in Eqs. (3.6) and (3.7) as follows:

$$T_s(r_0, t) = T_0, \quad r = r_0$$ (3.6)

and

$$T_s(r_0 - s(t), t) = T_{m,} \quad r = r_0 - s(t).$$ (3.7)

For simplicity, we set the melt bulk temperature to a constant C degrees higher than the interface temperature as stated in Eq. (3.8).

$$T_b - T_m = C$$ (3.8)

3.5 Dimensional Analysis

Since Eq. (3.1) is in cylindrical coordinates, it is extremely difficult to obtain a solution by directly solving the heat equation. However, we can solve the problem by using dimensional analysis. Besides the temperature in the governing equation, there are three other dimensional quantities in the system: thermal diffusivity α (units, m^2s^{-1}),

length r (unit, m), and time t (unit, s). If we consider the factor $\alpha^a r^b t^c$, the units will be $m^{2a+b} s^{-a+c}$. These will be dimensionless if $2a + b = -a + c = 0$. Thus, this leads to the ratio $a{:}b{:}c = -1{:}2{:}-1$. Any function of these will also be dimensionless, and it proves to be somewhat more convenient if the combination

$$\eta = \frac{r}{\sqrt{4\alpha t}}$$

(3.9)

is used instead[67]. These considerations suggest that the one-dimensional time-dependent conduction Eq. (3.1) has a solution of the following form:

$$T_s(x, t) = T_0 + (T_1 - T_0) f(\eta),$$

(3.10)

where T_0 is the initial temperature, and T_1 is the temperature at time t.

3.6 Problem Solutions

Since we already know the form of the solution, we can solve for the function $f(\eta)$ by substituting the solution into the governing equation and using the boundary conditions in Eqs. (3.6) - (3.8).

Using the chain rule of differentiation in Eq. (3.10), we obtain

$$\frac{\partial T_s}{\partial t} = (T_1 - T_0)\frac{df}{d\eta}\frac{d\eta}{dt} = (T_1 - T_0)\frac{df}{d\eta}\eta\left(-\frac{1}{2t}\right),$$

(3.11)

$$\frac{\partial T_s}{\partial r} = (T_1 - T_0)\frac{df}{d\eta}\frac{d\eta}{dr} = (T_1 - T_0)\frac{df}{d\eta}\frac{1}{\sqrt{4\alpha t}},$$

(3.12)

and

$$\frac{\partial T_s}{\partial r^2} = (T_1 - T_0)\frac{d^2 f}{d\eta^2}\frac{1}{4\alpha t}.$$

(3.13)

Substituting Eqs. (3.11)-(3.13) into Eq. (3.1), we obtain

$$\frac{d^2 f}{d\eta^2} + (2\eta + \frac{1}{\eta})\frac{df}{d\eta} = 0.$$ (3.14)

Integrating Eq. (3.14) twice gives the solution

$$\frac{df}{d\eta} = A\frac{1}{\eta} e^{-\eta^2}$$ (3.15)

$$f(\eta) = A\int_0^{\eta} \frac{1}{\xi} e^{-\xi^2} d\xi + B$$ (3.16)

where A and B are constants. By substituting back into Eq. (3.10), we obtain the solution

$$T_s(r,t) = A\int_0^{\frac{r}{\sqrt{4\alpha t}}} \tfrac{1}{\xi} e^{-\xi^2} d\xi + B.$$ (3.17)

Now, we solve for the constants A and B using the boundary and interface conditions.

Using Eqs. (3.2), (3.6), and (3.7), we obtain

$$-k_s A\frac{\sqrt{4\alpha t}}{r_0 - s(t)} e^{-\frac{(r_0 - s(t))^2}{4\alpha t}} \frac{1}{\sqrt{4\alpha t}} = \rho\lambda\frac{ds}{dt} + h_l(T_b(t) - T_m(t)),$$ (3.18)

$$T_0(t) = A\int_0^{\frac{r_0}{\sqrt{4\alpha t}}} \tfrac{1}{\xi} e^{-\xi^2} d\xi + B,$$ (3.19)

and

$$T_m(t) = A\int_0^{\frac{r_0 - s(t)}{\sqrt{4\alpha t}}} \tfrac{1}{\xi} e^{-\xi^2} d\xi + B.$$ (3.20)

In Eqs. (3.18)-(3.20), A and B are unknown. Also, solidification speed (ds/dt) and the wall temperature (T_0) are unknown. However, during solidification, we first specify one constant (solidification speed) and calculate the wall temperature, then we fix the wall temperature (at a certain value) and calculate crystal growth. These two stages go in sequence, so at any one time, there is only one unknown, solidification speed or wall temperature. As a result, we solve the problem using Eqs. (3.18) - (3.20).

Eliminating the constants, A and B, in Eqs. (3.18) - (3.20), we obtain

$$T_0(t) = T_m(t) - \frac{1}{k_s}\left[\rho\lambda\frac{ds}{dt} + h_l(Tb - Tm(t))\right](r_0 - s(t))\, e^{\frac{(r_0-s(t))^2}{4\alpha t}} \int_{\frac{r_0-s(t)}{\sqrt{4\alpha t}}}^{\frac{r_0}{\sqrt{4\alpha t}}} \frac{1}{\xi}e^{-\xi^2}d\xi . \quad (3.21)$$

This is the equation that relates the wall temperature T_0, to solidification speed ds/dt, interface temperature T_m, and time t. In what follows, we give the solutions for two solidification stages: solidification with a constant solidification speed, and solidification with a fixed wall temperature.

3.6.1 Solid Growth At Constant Speed

If the speed at which the solid layer grows is a constant u, we have $ds(t)/dt = u$ and hence $s(t) = ut$ with $s(0) = 0$. Substituting $s(t) = ut$ into Eq. (3.21), we obtain the surface temperature $T_0(t)$ profile at different times:

$$T_0(t) = T_m(t) - \frac{1}{k_s}\left[\rho\lambda u + h_l(T_b(t) - T_m(t))\right](r_0 - s(t))\, e^{\frac{(r_0-s(t))^2}{4\alpha t}} \int_{\frac{r_0-s(t)}{\sqrt{4\alpha t}}}^{\frac{r_0}{\sqrt{4\alpha t}}} \frac{1}{\xi}e^{-\xi^2}d\xi . \quad (3.22)$$

Here, $\lambda' = \lambda + C_{pl}(T_b - T_m)$, and the interface temperature $T_m(t)$ can be calculated through the Van Laar Eqs. (3.4) and (3.5),

$$T_m = \frac{1}{\dfrac{1}{T_A^f} - \dfrac{R}{\Delta H_A^f}\ln(X_{liquid})}, \qquad (3.23)$$

$$\text{where } X_{liquid} = \frac{r_0^2}{[r_0 - s(t)]^2}(X_{init} - X_S) + X_S. \qquad (3.24)$$

For simplicity, we choose $T_b(t)$ to be some constant degrees higher than $T_m(t)$.

To obtain the temperature distribution $T_s(r, t)$ within the solid, we subtract Eq. (3.19) from Eq. (3.20) to obtain

$$A = \frac{T_0(t) - T_m(t)}{Integral}, \quad where\, Integral = \int_{\frac{r_0-s(t)}{\sqrt{4\alpha t}}}^{\frac{r_0}{\sqrt{4\alpha t}}} \frac{1}{\xi}e^{-\xi^2}d\xi . \qquad (3.25)$$

By eliminating the constant B in Eqs. (3.17) and (3.19), one can solve for $T_s(r, t)$ to

obtain

$$T_s(r,t) \;=\; T_0 - A \int_{\frac{r}{\sqrt{4\alpha t}}}^{\frac{r_0}{\sqrt{4\alpha t}}} \tfrac{1}{\xi} e^{-\xi^2} d\xi \,.$$

(3.26)

3.6.2 Solid Growth after Wall
Temperature Reaches a Lower Limit

With time, $T_0(t)$ will drop to a temperature constraint imposed by the cooling

utilities. After the temperature reaches the operation limit, say T_0^c at time t^c, one may

hold the surface temperature at T_0^c and then let the solidification process continue with a

solid width of s^c. In this case, we substitute $T_0(t) = T_0^c$ into Eq. (3.21) and obtain a first-

order nonlinear ordinary differential equation as follows:

$$T_0^c \;=\; T_m(t) - \frac{1}{k_s}\Big[\rho\lambda' \tfrac{ds(t)}{dt} + h_l\big(T_b(t) - T_m(t)\big)\Big](r_0 - s(t))\, e^{\frac{(r_0 - s(t))^2}{4\alpha t}} \int_{\frac{r_0 - s(t)}{\sqrt{4\alpha t}}}^{\frac{r_0}{\sqrt{4\alpha t}}} \tfrac{1}{\xi} e^{-\xi^2} d\xi \,.$$

(3.27)

Using the implicit Euler method, equation (3.27) is then discretized as follows:

$$T_0^c \;=\; T_m^{n+1} - \frac{1}{k_s}\Big[\rho\lambda' \tfrac{s^{n+1}-s^n}{\Delta t} + h_l\big(T_b - T_m^{n+1}\big)\Big](r_0 - s^{n+1})\, e^{\frac{(r_0 - s^{n+1})^2}{4\alpha t_{n+1}}} \int_{\frac{r_0 - s^{n+1}}{\sqrt{4\alpha t_{n+1}}}}^{\frac{r_0}{\sqrt{4\alpha t_{n+1}}}} \tfrac{1}{\xi} e^{-\xi^2} d\xi \,,$$

(3.28)

where s^n is the approximation of $s(t_n)$, n is time level, and Δt is time increment. The initial

interface is set at $s(t_{n0})$, where t_{n0} is the time duration where the solid layer growth is a

constant. Since equation (3.28) is a nonlinear equation for s^{n+1}, we let

$$F(s^{n+1}) \equiv T_m^{n+1} - \frac{1}{k_s}\Big[\rho\lambda' \tfrac{s^{n+1}-s^n}{\Delta t} + h_l\big(T_b - T_m^{n+1}\big)\Big](r_0 - s^{n+1})\, e^{\frac{(r_0 - s^{n+1})^2}{4\alpha t_{n+1}}} \int_{\frac{r_0 - s^{n+1}}{\sqrt{4\alpha t_{n+1}}}}^{\frac{r_0}{\sqrt{4\alpha t_{n+1}}}} \tfrac{1}{\xi} e^{-\xi^2} d\xi - T_0^c \,.$$

(3.29)

Using Newton's iterative method, we can calculate the solid growth over time as

$$s_{new}^{n+1} \;=\; s_{old}^{n+1} - \frac{F(s_{old}^{n+1})}{F'(s_{old}^{n+1})},$$

(3.30)

where the integral in Eq. (3.29) is calculated by the composite Simpson's rule[68].

After the solid growth is achieved, one can calculate the temperature distribution in the solid layer by using the same method in section 3.6.1. This gives

$$T_s(r,t) \;=\; T_0 - A \int_{\frac{r}{\sqrt{4\alpha t}}}^{\frac{r_0}{\sqrt{4\alpha t}}} \tfrac{1}{\xi} e^{-\xi^2} d\xi, \quad where \; A \;=\; \frac{T_0(t)-T_m(t)}{\int_{\frac{r_0-s(t)}{\sqrt{4\alpha t}}}^{\frac{r_0}{\sqrt{4\alpha t}}} \tfrac{1}{\xi} e^{-\xi^2} d\xi}, \tag{3.31}$$

$$T_m \;=\; \frac{1}{\dfrac{1}{T_A^f} - \dfrac{R}{\Delta H_A^f} \ln(X_{liquid})}, \tag{3.32}$$

and

$$X_{liquid} \;=\; \frac{r_0^2}{[r_0 - s(t)]^2}\left(X_{init} - X_S\right) + X_S. \tag{3.33}$$

3.7 Algorithm

A procedure for predicting solid growth from melt crystallization can be written as follows:

Phase A. Given a constant speed u, solve the surface temperature $T_0(t)$ from Eq. (3.22) until it reaches the lower limit, $T_0(t_{n0}) = T_0^c$.

Phase B. Letting $T_0(t) = T_0^c$ and $s_{n0} = s(t_{n0})$, solve for s^{n+1} from equation (3.30), and continue iteration until the crystal growth rate falls below a threshold, $s^{n+1} - s^n < \varepsilon$.

The algorithm for solving the problem is listed below in detail:

Step 1: initialize dt, dr, $t=0$, ε, u, C.

Step2: increment time $t=t+dt$, $s = u^*t$.

Step 3: calculate the interface temperature T_m using Eq. (3.23).

Step 4: update the bulk temperature T_b using Eq. (3.8).

Step 5: calculate λ' using equation (3.3).

Step 6: calculate the wall temperature T_0 using Eq. (3.22).

Step 7: calculate the solid temperature distribution T_s using Eq. (3.26).

Step 8: check if $T_0 <= T_0^c$.

  If $T_0 <= T_0^c$,

     Continue with Step 9.

  Else,

     Continue with Step 2.

Step 9: increment time $t = t + dt$.

Step 10: calculate s^{n+1} using Eq. (3.30).

Step 11: calculate $\Delta r = s^{n+1} - s^n$.

Step 12: calculate the interface temperature T_m using Eq. (3.32).

Step 13: calculate the solid temperature distribution T_s using Eq. (3.31).

Step 14: check if $s^{n+1} - s^n < \varepsilon$.

  If $s^{n+1} - s^n < \varepsilon$,

     Stop.

  Else,

     Continue with Step 9.

CHAPTER FOUR

MODELING OF BINARY MELT CRYSTALLIZATION

WITH A LIQUID TEMPERATURE DISTRIBUTION

4.1 Introduction

Chapter three presents a numerical model to simulate melt crystallization in the case of a fully stirred binary melt. A more realistic scenario is the situation where the melt is not stirred. In such a case, the temperature of the melt decreases from the center to the solid-liquid interface. In this chapter, we present a model to simulate this situation.

The binary melt crystallization scheme to be modeled is illustrated in Fig. 4.1. Here, T_l is the liquid temperature, T_0 is the wall temperature, r_0 is the radius of the cylinder, and s is the solid layer width. The binary melt is preheated, in a temperature controlled cylindrical container, a few degrees higher than the eutectic temperature of the compound. Then, the melt is cooled down by decreasing the wall temperature T_0 of the cylindrical container causing one component to solidify. The solid layer grows from the wall towards the center of the container.

In this model, we assume that the liquid is still, in which case the melt temperature decreases from the center to the solid-liquid interface during the crystallization process. We also assume that the solid remains pure and all of the

42

impurities remain in the liquid. This is a reasonable assumption for eutectic systems as

long as the solidification speed does not exceed a certain threshold [69].
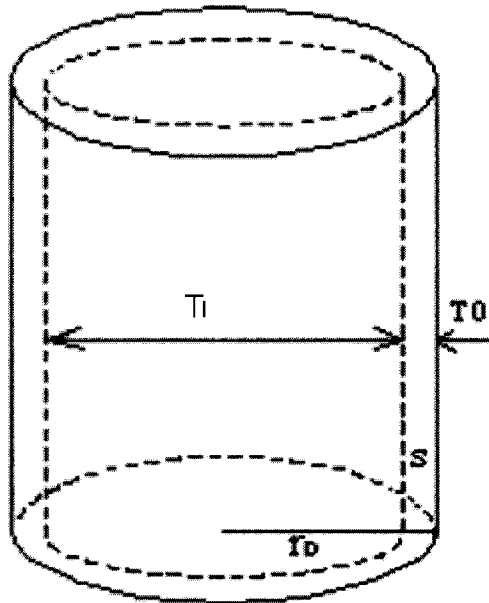
Figure 4.1 Schematic view of a three-dimensional
solidification problem
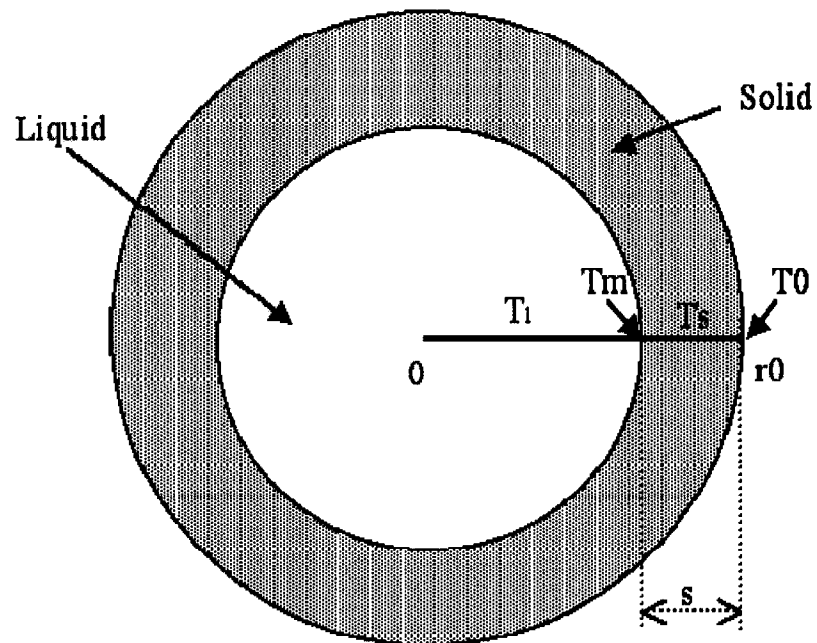
Figure 4.2 Simplified two-dimensional
binary melt crystallization scheme

Under certain assumptions, one may simplify the problem to one-dimension. First, assume that the ratio of the length of the cylinder to its radius is large enough so that one can simplify the model from three-dimensions to two-dimensions as described in Fig. 4.2. Here, T_m is the interface temperature, and T_s is the solid temperature.

Since the two-dimensional problem in Fig. 4.2 is circularly symmetric, one can simplify the problem further to one-dimension as illustrated in Fig. 4.3.
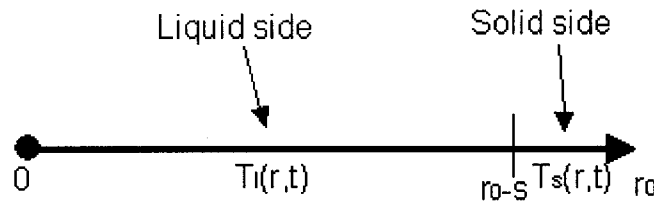
Figure 4.3 Simplified one-dimensional scheme

A solution to the one-dimensional problem involves solving for the temperature distribution along the radius of the cylinder. The difference of the simplified problem in this model with the previous one is that the previous model solves for the temperature distribution along the solid part ($r_0\text{-}s<r<=r_0$), and this model solves for the whole temperature distribution, solid and liquid ($0<r<=r_0$). In this chapter, in addition to the solid governing equations, we will introduce the liquid governing equations. Also, an interface equation and liquid boundary equation will be introduced.

4.2 Solid and Liquid Governing Equations

For the solid layer and liquid bulk, the heat transfer equations are given as

$$\frac{1}{\alpha_s}\frac{\partial T_s}{\partial t} = \frac{1}{r}\frac{\partial}{\partial r}(r\frac{\partial T_s}{\partial r}), \quad r_0 - s(t) < r < r_0, \tag{4.1}$$

and

$$\frac{1}{\alpha_l}\frac{\partial T_l}{\partial t} = \frac{1}{r}\frac{\partial}{\partial r}(r\frac{\partial T_l}{\partial r}), \quad 0 < r < r_0 - s(t), \tag{4.2}$$

where T_s and T_l are the temperatures in the solid and liquid, respectively, α_s and α_l are the heat diffusivities within the solid and liquid phases, $s(t)$ is the solid layer thickness, and r_0 is the radius of the cylinder.

4.3 Solid-Liquid Interface Equation

The solid-liquid interfacial equation is given as

$$-L\frac{ds(t)}{dt} = k_s\left(\frac{\partial T_s}{\partial r}\right) - k_l\left(\frac{\partial T_l}{\partial r}\right), \quad r = r_0 - s(t), \tag{4.3}$$

where L is the latent heat per unit volume of solid, k_s and k_l are the heat conductivity coefficients of the solid and liquid layer, respectively, T_l is temperature of the melt, and T_s is the temperature of the solid crystal layer.

4.4 Boundary Conditions

It is assumed that the wall temperature T_0 is equal to the temperature of the solid at the point $r=r_0$. The temperatures of the solid and liquid at the interface ($r=r_0-s(t)$) are both equal to the interface temperature, T_m. These boundary conditions are described in Eqs. (4.4)-(4.6) as follows:

$$T_s(r_0,t) = T_0, \tag{4.4}$$

$$T_s(r_0 - s(t),t) = T_m, \tag{4.5}$$

and

$$T_l(r_0 - s(t),t) = T_m. \tag{4.6}$$

In Eqs. (4.5) and (4.6), T_m is the melting temperature as determined by the Van Laar equation

$$\ln(X_{liquid}) = \frac{\Delta H_A^f}{R}(\frac{1}{T_A^f} - \frac{1}{T_m}),$$

(4.7)

where $X_{liquid} = \frac{r_0^2}{[r_0 - s(t)]^2}(X_{init} - X_S) + X_S.$

(4.8)

Here, X_{init} is the initial composition of the compound, and X_s is the composition of the solid.

At the center of the melt, the temperature distribution is axi-symmetric, and there is no heat diffusion across the center. This means that the temperature derivative is zero at that point. Thus, we obtain the following boundary condition,

$$\frac{\partial T_l}{\partial r} = 0, \quad r = 0.$$

(4.9)

4.5 Mathematical Model

We first give the mathematical model for the melt side. Then by adding the interface equation, we will solve the temperature distribution for the solid side.

4.5.1 Solution in the Melt Phase

The interface temperature is actually the melting point of the compound, and it is only related to the composition of the compound. For a given initial composition, since the solid is pure by assumption, the composition of the compound at a given time is only related to the solid width. The more the target component has been solidified out, the lower the composition of the component in the melt. This is obvious from the Van Laar

equation. By solving Eqs. (4.7) and (4.8), we can calculate T_m for the given solid layer

width, $s(t)$:

$$T_m = \cfrac{1}{\cfrac{1}{T_A^f} - \cfrac{R}{\Delta H_A^f}\ln(X_{liquid})}, \tag{4.10}$$

$$\text{where } X_{liquid} = \frac{r_0^2}{[r_0 - s(t)]^2}(X_{init} - X_S) + X_S. \tag{4.11}$$

To obtain the temperature distribution of the melt, we solve the governing equation

(4.2) with the boundary condition at the interface, which is T_m in equation (4.10), and the

boundary condition at the center in equation (4.9). Figure 4.4 illustrates the grid points

used in the numerical solution.
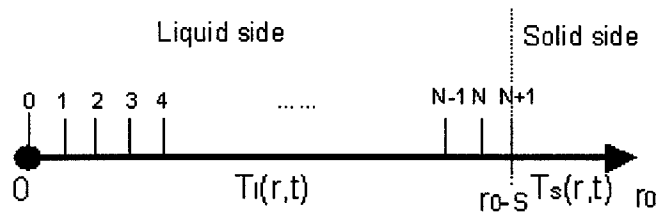
Figure 4.4 Grid points

Because of the growth of the solid layer, the interface point $T_l(r,t)|_{N+1}$ will move

inward causing the number of grid points to decrease. At a given time level $n+1$, we have

$$T_l\big|_{N+1}^{n+1} = T_m \tag{4.12}$$

by equation (4.6). By discretizing equation (4.9), we have

$$\frac{T_l\big|_0^{n+1} - T_l\big|_1^{n+1}}{\Delta r} = 0, \tag{4.13}$$

or

$$T_l\big|_0^{n+1} = T_l\big|_1^{n+1}. \tag{4.14}$$

By discretizing equation (4.2), we have

$$\frac{1}{\alpha_l}\frac{T_l\big|_j^{n+1}-T_l\big|_j^{n}}{\Delta t} = \frac{1-\theta}{r_j}\frac{1}{\Delta r^2}\left[r_{j+\frac{1}{2}}\left(T_l\big|_{j+1}^{n+1}-T_l\big|_j^{n+1}\right)-r_{j-\frac{1}{2}}\left(T_l\big|_j^{n+1}-T_l\big|_{j-1}^{n+1}\right)\right]$$

$$+ \frac{\theta}{r_j}\frac{1}{\Delta r^2}\left[r_{j+\frac{1}{2}}\left(T_l\big|_{j+1}^{n}-T_l\big|_j^{n}\right)-r_{j-\frac{1}{2}}\left(T_l\big|_j^{n}-T_l\big|_{j-1}^{n}\right)\right]. \qquad (4.15)$$

Here, θ is the distribution factor for this implicit scheme.

Equations (4.12), (4.14), and (4.15) form a tridiagonal linear system.

$$\begin{bmatrix} -a_1+b_1 & -c_1 & & & \\ -a_2 & b_2 & -c_2 & & \\ & \cdots & \cdots & \cdots & \\ & & -a_{N-1} & b_{N-1} & -c_{N-1} \\ & & & -a_N & b_N \end{bmatrix}\begin{bmatrix} T_l\big|_1^{n+1} \\ T_l\big|_2^{n+1} \\ \cdots \\ T_l\big|_{N-1}^{n+1} \\ T_l\big|_N^{n+1} \end{bmatrix} = \begin{bmatrix} d_1 \\ d_2 \\ \cdots \\ d_{N-1} \\ d_N+c_N T_m \end{bmatrix} \qquad (4.16)$$

where,

$$a_j = (1-\theta)r_{j-\frac{1}{2}}$$

$$b_j = 2(1-\theta)r_j + \frac{\Delta r^2}{\alpha_2\Delta t}r_j$$

$$c_j = (1-\theta)r_{j+\frac{1}{2}} \qquad (4.17)$$

$$d_j = \theta\, r_{j-\frac{1}{2}}T_l\big|_{j-1}^{n} + \left(\frac{\Delta r^2}{\alpha_2\Delta t}r_j - 2\theta\, r_j\right)T_l\big|_j^{n} + \theta\, r_{j+\frac{1}{2}}T_l\big|_{j+1}^{n}$$

$$j = 1,2,...N,$$

and

$$r_j = r_0 - s(t) + j\Delta t$$

$$r_{j-\frac{1}{2}} = r_0 - s(t) + (j-\tfrac{1}{2})\Delta t$$

$$r_{j+\frac{1}{2}} = r_0 - s(t) + (j+\tfrac{1}{2})\Delta t .$$

Using Gaussian elimination, we obtain the melt temperatures $T_l|_j^{n+1}$, $j=0, 1, ...,$

$N+1$. These values are taken to the next time level $T_l|_j^n$, and some points are

automatically discarded because the interface moves.

It should be pointed out that through this process, the obtained solution is a

function of the solid width $s(t)$. When the solidification has a constant speed u, the solid

width is equal to ut. After the wall temperature reaches a fixed point, the solid width can

be calculated using the iteration method introduced in the following section.

4.5.2 Solution in the Solid Phase

After calculating the liquid side temperatures, one has $T_l|_N^{n+1}$ and $T_l|_{N+1}^{n+1}$. Hence, the

term $\dfrac{\partial T_l}{\partial r}$ in the interface equation (4.3) can be calculated as $\dfrac{T_l|_N^{n+1} - T_l|_{N+1}^{n+1}}{\Delta r}$.

By using dimensional analysis as in Chapter Three, we can construct a

dimensionless variable η to combine the three dimensional variables in the system:

thermal diffusivity α (units, $m^2 s^{-1}$), length r (unit, m), and time t (unit, s). The variable η

is given as

$$\eta = \frac{r}{\sqrt{4\alpha t}}. \tag{4.18}$$

The one-dimensional time-dependent conduction equation (4.1) has a solution of

the form

$$T_s(x, t) = T_0 + (T_1-T_0)f(\eta), \tag{4.19}$$

where T_0 is the initial temperature, and T_1 is the temperature at time t.

One can solve for the function $f(\eta)$ by substituting the solution from Eq. (4.19) into the governing equation and using the boundary conditions. Using the chain rule of differentiation in equation (4.19), one obtains

$$\frac{\partial T_s}{\partial t} = (T_1 - T_0)\frac{df}{d\eta}\frac{d\eta}{dt} = (T_1 - T_0)\frac{df}{d\eta}\eta\left(-\frac{1}{2t}\right),$$

(4.20)

and

$$\frac{\partial T_s}{\partial r} = (T_1 - T_0)\frac{df}{d\eta}\frac{d\eta}{dr} = (T_1 - T_0)\frac{df}{d\eta}\frac{1}{\sqrt{4\alpha t}}.$$

(4.21)

As such,

$$\frac{\partial T_s}{\partial r^2} = (T_1 - T_0)\frac{d^2 f}{d\eta^2}\frac{1}{4\alpha t}.$$

(4.22)

Substituting Eqs. (4.20)-(4.22) into Eq. (4.1), we obtain

$$\frac{d^2 f}{d\eta^2} + (2\eta + \frac{1}{\eta})\frac{df}{d\eta} = 0.$$

(4.23)

Integrating Eq. (4.23) twice gives the solution

$$\frac{df}{d\eta} = A'\frac{1}{\eta}\,e^{-\eta^2},$$

(4.24)

and

$$f(\eta) = A'\int_0^\eta \frac{1}{\xi}e^{-\xi^2}\,d\xi + B',$$

(4.25)

where A' and B' are constants. By substituting back into equation (4.19), we obtain the solution to the problem,

$$T_s(r,t) = A\int_0^{\frac{r}{\sqrt{4\alpha t}}} \frac{1}{\xi}e^{-\xi^2}\,d\xi + B.$$

(4.26)

Here A and B are constants. Now, we solve for A and B using the boundary and interface conditions.

Using Eqs. (4.3), (4.4), and (4.5), we obtain

$$-Lu = k_s A \frac{\sqrt{4\alpha t}}{r_0 - ut} e^{-\frac{(r_0 - ut)^2}{4\alpha t}} \frac{1}{\sqrt{4\alpha t}} - k_l \left(\frac{\partial T_l}{\partial r}\right), \quad where \ r = ut, \quad (4.27)$$

$$T_0(t) = A \int_0^{\frac{r_0}{\sqrt{4\alpha t}}} \frac{1}{\xi} e^{-\xi^2} d\xi + B, \quad (4.28)$$

and

$$T_m(t) = A \int_0^{\frac{r_0 - s(t)}{\sqrt{4\alpha t}}} \frac{1}{\xi} e^{-\xi^2} d\xi + B. \quad (4.29)$$

In Eq. (4.27), the term $\dfrac{\partial T_l}{\partial r}$ is known as $\dfrac{T_l\big|_N^{n+1} - T_l\big|_{N+1}^{n+1}}{\Delta r}$ from the solution of the liquid temperature. In Eqs. (4.27)-(4.29), A, B, solidification speed, ds/dt, and wall temperature T_0, are unknowns. However, during solidification, we first specify one constant (solidification speed) and calculate the wall temperature. Then, we fix the wall temperature (at a certain value) and calculate solid growth. These two stages go in sequence, so at any one time, there is only one unknown, solidification speed or wall temperature. As a result, we solve the problem using Eqs. (4.27) - (4.29).

Eliminating the constants A and B in Eqs. (4.27)-(4.29), we obtain

$$T_0(t) = T_m(t) + \frac{r_0 - s(t)}{k_s} \left(-L\frac{ds}{dt} + k_l \frac{\partial T_l}{\partial r}\right) e^{\frac{(r_0 - s)^2}{4\alpha t}} \int_{\frac{r_0 - s}{\sqrt{4\alpha t}}}^{\frac{r_0}{\sqrt{4\alpha t}}} \frac{1}{\xi} e^{-\xi^2} d\xi. \quad (4.30)$$

This is the equation that relates the wall temperature T_0 to the solidification speed ds/dt, the interface temperature T_m, and time t. In what follows, we give solutions for two solidification cases: solidification under a constant speed, and solidification under a fixed wall temperature.

4.5.2.1 Solid Growth at a Constant Speed. In this case, we first calculate the liquid

phase temperature by solving the linear system as introduced in section 4.5.1. Then, from

the liquid temperatures at the interface $T_l\big|_N^{n+1}$ and $T_l\big|_{N+1}^{n+1}$, $\dfrac{\partial T_l}{\partial r}$ can be calculated as

$\dfrac{T_l\big|_N^{n+1} - T_l\big|_{N+1}^{n+1}}{\Delta r}$. If the solid layer grows at a constant speed u, then $ds(t)/dt = u$ and $s(t) = ut$

with $s(0) = 0$. Replacing $s(t)$ by ut and $\dfrac{\partial T_l}{\partial r}$ by $\dfrac{T_l\big|_N^{n+1} - T_l\big|_{N+1}^{n+1}}{\Delta r}$ in equation (4.30), one

obtains the surface temperature $T_0(t)$ profile over time,

$$T_0(t) = T_m(t) + \frac{r_0 - s(t)}{k_s}\left(-Lu + k_l \frac{T_l\big|_N^{n+1} - T_l\big|_{N+1}^{n+1}}{\Delta r}\right) e^{\frac{(r_0 - s(t))^2}{4\alpha t}} \int_{\frac{r_0 - s(t)}{\sqrt{4\alpha t}}}^{\frac{r_0}{\sqrt{4\alpha t}}} \frac{1}{\xi} e^{-\xi^2} d\xi. \tag{4.31}$$

To obtain the temperature distribution $T_s(r, t)$ within the solid, we subtract Eq.

(4.28) from Eq. (4.29) to give

$$A = \frac{T_0(t) - T_m(t)}{Integral}, \quad where\, Integral = \int_{\frac{r_0 - s(t)}{\sqrt{4\alpha t}}}^{\frac{r_0}{\sqrt{4\alpha t}}} \frac{1}{\xi} e^{-\xi^2} d\xi. \tag{4.32}$$

Subtracting Eq. (4.26) from Eq. (4.28), one obtains

$$T_s(r,t) = T_0 - A \int_{\frac{r}{\sqrt{4\alpha t}}}^{\frac{r_0}{\sqrt{4\alpha t}}} \frac{1}{\xi} e^{-\xi^2} d\xi. \tag{4.33}$$

4.5.2.2 Solid Growth after the Wall Temperature Reaches a Lower Limit. When

the wall temperature reaches a certain fixed point, the solid layer growth slows down as

time proceeds. We first calculate the solid layer growth for the next time step using

iteration, then calculate the liquid temperature distribution using the method in section

4.5.1. At last, we will derive the analytic solution for the solid phase.

With time, $T_0(t)$ will drop to a point imposed by the cooling utilities. After the

temperature reaches this point, say T_0^c at time t^c, and the solid layer width reaches s^c, one

may hold the surface temperature at $T_0{}^c$ and then let the solidification process continue

with the initial width s^c. In this case, the liquid temperatures at the interface $T_l|_N^n$ and

$T_l|_{N+1}^n$ are known. By discretizing $\dfrac{\partial T_l}{\partial r}$ to $\dfrac{T_l|_N^n - T_l|_{N+1}^n}{\Delta r}$, we replace $T_0(t)$ by $T_0{}^c$ and $\dfrac{\partial T_l}{\partial r}$

by $\dfrac{T_l|_N^n - T_l|_{N+1}^n}{\Delta r}$ in Eq. (4.30) to obtain the first-order nonlinear ordinary differential

equation:

$$T_0{}^c = T_m(t) + \frac{r_0 - s(t)}{k_s}\left(-L\frac{ds}{dt} + k_l \frac{T_l|_N^n - T_l|_{N+1}^n}{\Delta r}\right) e^{\frac{(r_0 - s)^2}{4\alpha t}} \int_{\frac{r_0 - s}{\sqrt{4\alpha t}}}^{\frac{r_0}{\sqrt{4\alpha t}}} \frac{1}{\xi} e^{-\xi^2}\, d\xi . \qquad (4.34)$$

Since the wall temperature is fixed, the solidification speed $\dfrac{ds}{dt}$ is no longer a

constant. In order to solve for the solid layer growth at the next time level, we discretize

$\dfrac{ds}{dt}$ as $\dfrac{\Delta s}{\Delta t}$. Since calculation of the liquid phase temperature distribution uses fixed grid

points, $T_l|_i^{n+1}$ are dependent on the values of $T_l|_j^n$ for $i, j = 0,1,\ldots,N$. This requires that Δs

should be fixed. In order to calculate t^{n+1} for solid growth with fixed Δs, we construct a

function $f(s, t)$, and let

$$f(s,t) = \frac{dt}{ds} \qquad (4.35)$$

or

$$\frac{1}{f(s,t)} = \frac{ds}{dt}. \qquad (4.36)$$

By substituting Eq. (4.36) into Eq. (4.34), we solve for $f(s, t)$ and obtain

$$f(s,t) = \cfrac{L}{\cfrac{k_s(T_m(t)-T_0^c)}{(r_0-s(t))\int_{\frac{r_0-s}{\sqrt{4\alpha t}}}^{\frac{r_0}{\sqrt{4\alpha t}}}\frac{1}{x}e^{-x^2}dx}e^{-\frac{(r_0-s)^2}{4\alpha t}}+k_l\frac{T_l|_N^n-T_l|_{N+1}^n}{\Delta r}} \qquad (4.37)$$

Using the 4$^{\text{th}}$ order Runge-Kutta method, one obtains the solution,

$$t_{i+1} = t_i + \tfrac{1}{6}(k_1+2k_2+2k_3+k_4), \quad i=0,1,2,..,M, \qquad (4.38)$$

where

$$
\begin{aligned}
k_1 &= h\,f(s_i,t_i) \\
k_2 &= h\,f(s_i+\tfrac{h}{2},t_i+\tfrac{k_1}{2}) \\
k_3 &= h\,f(s_i+\tfrac{h}{2},t_i+\tfrac{k_2}{2}) \\
k_4 &= h\,f(s_i+h,t_i+k_3) \\
t_0 &= t^n, \quad s_0 = s^n \\
h &= \frac{\Delta s}{M}.
\end{aligned}
\qquad (4.39)
$$

As such, the next time level t^{n+1} for growth of the next solid layer is equal to t_M.

After solid growth is achieved, one can calculate the liquid temperature distribution $T_l|_j^{n+1}$, $j=0,1,...,N+1$. $T_l|_N^{n+1}$ and $T_l|_{N+1}^{n+1}$ will be used in the next time level for calculating growth of the solid layer. Then, one can solve for the temperature distribution in the solid phase by using the same method in section 4.5.2.1,

$$T_s(r,t) = T_0 - A\int_{\frac{r}{\sqrt{4\alpha t}}}^{\frac{r_0}{\sqrt{4\alpha t}}}\frac{1}{\xi}e^{-\xi^2}d\xi, \quad where\ A = \frac{T_0(t)-T_m(t)}{\int_{\frac{r_0-s(t)}{\sqrt{4\alpha t}}}^{\frac{r_0}{\sqrt{4\alpha t}}}\frac{1}{\xi}e^{-\xi^2}d\xi} \qquad (3.40)$$

and

$$T_m = \cfrac{1}{\cfrac{1}{T_A^f}-\cfrac{R}{\Delta H_A^f}\ln(X_{liquid})}, \qquad (3.41)$$

where

$$X_{liquid} = \frac{r_0^2}{[r_0-s(t)]^2}(X_{init}-X_S)+X_S. \qquad (3.42)$$

4.6 Algorithm

A procedure for predicting solid growth from melt crystallization can be written as follows:

Phase A. Given a constant speed u, calculate the liquid phase temperature distribution by solving the linear system in Eqs. (4.16)-(4.17). Then, by coupling with the interface equation, solve for the solid layer temperature distribution and the surface (wall) temperature $T_0(t)$ until it reaches the constraint, $T_0(t_{n0}) = T_0^c$.

Phase B. Fix the wall temperature T_0 at T_0^c. Fix Δs and set $s_{n0} = s(t_{n0})$. Solve for t^{n+1} using the 4th order Runge-Kutta method, then calculate the liquid side temperature distribution by solving the linear system of Eqs. (4.16)-(4.17) as in phase A. Then, by coupling with the interface equation, solve for the solid layer temperature distribution. Continue with the next solid growth until the solid growth rate falls below a threshold.

The steps for solving this problem are listed below:

Step 1: initialize Δt, Δr, $t=0$, ε, u, C.

Step2: increment time $t=t+\Delta t$, $s = u^*t$;

Step 3: calculate the interface temperature T_m using Eqs. (4.10) and (4.11).

Step 4: calculate the melt temperature T_l by solving the linear system in Eqs. (4.16)-(4.17).

Step 5: calculate $\dfrac{\partial T_l}{\partial r}$ by $\dfrac{T_l|_N^{n+1} - T_l|_{N+1}^{n+1}}{\Delta r}$.

Step 6: calculate the wall temperature T_0 using Eq. (4.31).

Step 7: calculate the solid temperature distribution T_s using Eqs. (4.32) and

(4.33).

Step 8: check if $T_0 <= T_0^c$.

If $T_0 <= T_0^c$,

Fix the wall temperature at T_0.

Continue with Step 9.

Else,

Continue with Step 2.

Step 9: increment solid growth $s = s + \Delta r$.

Step 10: calculate t^{n+1} using Eqs. (4.37)-(4.39).

Step 11: calculate $\Delta t = t^{n+1} - t^n$, and $c = \dfrac{\Delta r}{\Delta t}$.

Step 12: calculate the interface temperature T_m using Eqs. (4.10) and (4.11).

Step 13: calculate the melt temperature T_l by solving the linear system in Eqs.

(4.16)-(4.17).

Step 14: calculate $\dfrac{\partial T_l}{\partial r}$ by $\dfrac{T_l|_N^{n+1} - T_l|_{N+1}^{n+1}}{\Delta r}$.

Step 15: calculate the solid temperature distribution T_s using Eqs. (4.40)-(4.42).

Step 16: check if $c < \varepsilon$.

If $c < \varepsilon$

Stop.

Else,

Continue with Step 9.

CHAPTER FIVE

MODEL APPLICATION

This chapter presents specifications and requirements for applications of the two models developed in Chapters Three and Four. One application on separation via melt crystallization of para-dichlorobenzen from binary compound of two isomers (para-dichlorobenzen and ortho-dichlorobenzen) will be given. Parameters adopted for the models and the intermediate variables calculated will be described.

5.1 Application Requirements of the Models

The simplified model built in Chapter 3 and the complete model built in Chapter 4 are based on certain specifications including the kind of devices that should be used, and the kind of substances that can be separated. Whether or not a process follows model specifications will determine the success of the application of the model.

5.1.1 Utilities

The two models in Chapter 3 and Chapter 4 give solutions for one-dimensional solidification problems as illustrated in Figures 3.1 and 4.1. As explained in Chapter 3 and Chapter 4, the simplification from three- to one-dimension requires that the ratio of the length of the cylinder to its diameter should be large, and the cylinder should be circular and symmetric.

57

The models deal with the inverse heat conduction problem. The output of the models is the wall temperature profile for a constant solidification speed and solid layer growth after the wall temperature reaches a lower limit. The temperature distribution in the solid (simplified model) or the temperature distributions in both solid and liquid (extended model) will be calculated to demonstrate the solidification process.

The simplified model in Chapter 3 is based on the assumption that the bulk temperature is constant with no gradient along the radius of the cylindrical crystallizer. This requires that the melt should be evenly mixed during the solidification process.

The extended model in Chapter 4 allows for a radial temperature gradient in both the solid and liquid phases. In this case, the melt has a temperature distribution which decreases from the center to the interface.

5.1.2 Components of the Compound

In this study, we model solid layer growth from melt crystallization in the case of a binary compound. The component in the solid layer is pure and the melt contains the binary compound. Systems with more than two components typically behave similarly to binary systems if the components do not interact with each other.

It is assumed that the two components are not miscible, thus forming a eutectic system (see Chapter 2 for details). Eutectic behavior is necessary for solid layer growth from melt crystallization. Consider the example in Fig. 2.1 with two components, A and B. If one wishes to separate component B from the A, B mixture, the initial composition of B should fall on the right side of the eutectic point (E), that is, it should be larger than X_E. Otherwise, component A will be solidified out first.
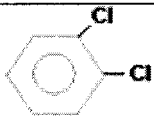
The models developed in this study are more suitable for the separation of organic compounds which are usually difficult to separate using some other techniques.

5.2 Model Application

5.2.1 Selection of the Compound

To test our combined analytic and numerical method, we employ the models to simulate the inward solidification of para-dichlorobenzene from the binary ortho-dichlorobenzene (ODCB) and para-dichlorobenzene (PDCB) compound. This compound is an isomeric mixture (Table 5.1) that is of significance in industry. It is a good candidate for melt crystallization due to the serious challenges that separation via distillation would present.

Table 5.1. Technical specifications of the two components, ODCB and PDCB[72].

Chemical Name	Orthodichlorobenzene	Paradichlorobenzene
Molecular Formula	$C_6H_4Cl_2$	$C_6H_4Cl_2$
Molecular Weight	147.00	147.00
CAS Registry Number	95-50-1	106-46-7
Chemical Structure		
Other Names	1, 2 - Dichlorobenzene, ODCB, O-Dichlorobenzene	1, 4 - Dichlorobenzene, PDCB, P-Dichlorobenzene

Ortho-dichlorobenzene is used primarily in the synthesis of 3,4-dichloroaniline, which is used in the production of herbicides. It is also used in the manufacture of dyes, as a solvent in paint removers and engine cleaners, and as a de-inking solvent. Para-

dichlorobenzene is used in the manufacture of 1,2,4-trichlorobenzene, polyphenylene (Polyphenylene is a commercial polymer known as Ryton®, having many industrial applications[70]), sulfide resins, room deodorants, moth proofing products, and as an intermediate in the dye and insecticide industries[71].

5.2.2 Parameter Settings

In order to better describe the parameters of the system, we list the governing equations and boundary conditions for the models as described in Chapters 3 and 4.

For the simplified model in Chapter 3, the equations are

$$\frac{1}{\alpha}\frac{\partial T_s}{\partial t} = \frac{1}{r}\frac{\partial}{\partial r}(r\frac{\partial T_s}{\partial r}), \quad r_0 - s(t) < r < r_0, \tag{5.1}$$

$$-k_s\left(\frac{\partial T_s}{\partial r}\right) = \rho\lambda'\frac{ds(t)}{dt} + h_l(T_b - T_m), \quad r = r_0 - s(t), \tag{5.2}$$

$$T_s(r_0, t) = T_0, \quad r = r_0, \tag{5.3}$$

$$T_s(r_0 - s(t), t) = T_m, \quad r = r_0 - s(t), \tag{5.4}$$

$$\lambda' = \lambda + C_{pl}(T_b - T_m), \tag{5.5}$$

$$T_b - T_m = C. \tag{5.6}$$

For the complete model in Chapter 4, the equations are

$$\frac{1}{\alpha_s}\frac{\partial T_s}{\partial t} = \frac{1}{r}\frac{\partial}{\partial r}(r\frac{\partial T_s}{\partial r}), \quad r_0 - s(t) < r < r_0, \tag{5.7}$$

$$\frac{1}{\alpha_l}\frac{\partial T_l}{\partial t} = \frac{1}{r}\frac{\partial}{\partial r}(r\frac{\partial T_l}{\partial r}), \quad 0 < r < r_0 - s(t), \tag{5.8}$$

$$-L\frac{ds(t)}{dt} = k_s\left(\frac{\partial T_s}{\partial r}\right) - k_l\left(\frac{\partial T_l}{\partial r}\right), \quad r = r_0 - s(t), \tag{5.9}$$

$$T_s(r_0, t) = T_0, \tag{5.10}$$

$$T_s(r_0 - s(t), t) = T_m,$$ (5.11)

$$T_l(r_0 - s(t), t) = T_m,$$ (5.12)

$$\frac{\partial T_l}{\partial r} = 0, \quad r = 0.$$ (5.13)

Of the two models, the interface temperature T_m is calculated by the Van Laar Equation,

$$\ln(X_{liquid}) = \frac{\Delta H_A^f}{R}(\frac{1}{T_A^f} - \frac{1}{T_m})$$ (5.14)

where

$$X_{liquid} = \frac{r_0^2}{[r_0 - s(t)]^2}(X_{init} - X_S) + X_S.$$ (5.15)

In Eqs. (5.1)-(5.15), the radius of the cylinder r_0 is taken as 60mm. The heat diffusivity of the solid α and α_s in Eqs. (5.1) and (5.7), and the heat diffusivity of the liquid α_l in Equation (5.8) are calculated in the next section. In Eqs. (5.2) and (5.9), the thermal conductivity of PDCB (k_s) is 0.14473W/mK. In Equation (5.2), the solid density of PDCB (ρ) is 1.241kg/m^3. λ' is calculated from Eq. (5.5), and the heat convection coefficient (h_l) is 150W/mK. In Eq. (5.5), the heat released from crystallization (λ) is 18,160J/g·mole, and the specific heat (C_{pl}) is 170.9J/g·mole. The constant in Eq. (5.6) is taken as 1. In Eq. (5.9), the latent heat per unit volume of solid (L) and the heat conductivity of liquid (k_l) are calculated in the next section.

In Eqs. (5.14) and (5.15), because we assume that the solid is pure, the composition of the solid X_s is 1. The gas constant R is 8.32J/gmoleK. The molar heat of fusion ΔH_A^f and the liquidus temperature of the two components, oDCB and pDCB, are 12930J/gmole, 18160J/gmole, and 256K, 326.1K, respectively. The initial composition of

pDCB in the melt (X_{init}) is considered to be 0.95 or 0.8. Table 5.2 summarizes some of the parameters used in the models.

Table 5.2. Parameters used in applications of the models[73-74]

NAME	UNIT	VALUE
r_0	mm	60
$k_s(PDCB)$	W/mK	0.14473
$k_l(PDCB)$	W/mK	0.105
$k_l(ODCB)$	W/mK	0.121
$C_{pl}(PDCB)$	J/gK	1.188(liquid), 1.005(solid)
$C_{pl}(ODCB)$	J/gK	1.159(liquid)
$\rho(PDCB)$	kg/L	1.2475(liquid), 1.241(solid)
$\rho(ODCB)$	kg/L	1.3022(liquid)
h_l	W/mK	150
λ	J/g·mole	18,160
C	K	1
R	J/gmoleK	8.32
X_s	N/A	1
X_{init}	N/A	0.95, 0.8
$T_a^f(PDCB)$	K	326.1
$T_a^f(ODCB)$	K	256
$\Delta H^f_{us}(PDCB)$	J/gmole	18,160
$\Delta H^f_{us}(ODCB)$	J/gmole	12,930

The solution to the simplified model is as follows:

When the solidification speed is fixed, the wall temperature profile is

$$T_0(t) = T_m(t) - \frac{1}{k_s}\left[\rho\lambda u + h_l(T_b(t) - T_m(t))\right](r_0 - s(t)) e^{\frac{(r_0 - s(t))^2}{4\alpha t}} \int_{\frac{r_0 - s(t)}{\sqrt{4\alpha t}}}^{\frac{r_0}{\sqrt{4\alpha t}}} \frac{1}{\xi} e^{-\xi^2} d\xi . \quad (5.16)$$

The solid temperature distribution is

$$T_s(r,t) = T_0 - A \int_{\frac{r}{\sqrt{4\alpha t}}}^{\frac{r_0}{\sqrt{4\alpha t}}} \frac{1}{\xi} e^{-\xi^2} d\xi , \quad (5.17)$$

where

$$A = \frac{T_0(t) - T_m(t)}{Integral}, \text{ and the } integral = \int_{\frac{r_0 - s(t)}{\sqrt{4\alpha t}}}^{\frac{r_0}{\sqrt{4\alpha t}}} \frac{1}{\xi} e^{-\xi^2} d\xi . \quad (5.18)$$

When the wall temperature is fixed, solid growth is given by

$$s_{new}^{n+1} = s_{old}^{n+1} - \frac{F(s_{old}^{n+1})}{F'(s_{old}^{n+1})}, \quad (5.19)$$

where

$$F(s^{n+1}) \equiv T_m^{n+1} - \frac{1}{k_s}\left[\rho\lambda'\frac{s^{n+1} - s^n}{\Delta t} + h_l(T_b - T_m^{n+1})\right](r_0 - s^{n+1}) e^{\frac{(r_0 - s^{n+1})^2}{4\alpha t_{n+1}}} \int_{\frac{r_0 - s^{n+1}}{\sqrt{4\alpha t_{n+1}}}}^{\frac{r_0}{\sqrt{4\alpha t_{n+1}}}} \frac{1}{\xi} e^{-\xi^2} d\xi - T_0^c .$$

$$(5.20)$$

The solid temperature distribution is

$$T_s(r,t) = T_0 - A \int_{\frac{r}{\sqrt{4\alpha t}}}^{\frac{r_0}{\sqrt{4\alpha t}}} \frac{1}{\xi} e^{-\xi^2} d\xi, \quad where \ A = \frac{T_0(t) - T_m(t)}{\int_{\frac{r_0 - s(t)}{\sqrt{4\alpha t}}}^{\frac{r_0}{\sqrt{4\alpha t}}} \frac{1}{\xi} e^{-\xi^2} d\xi} . \quad (5.21)$$

In Eqs. (5.16)-(5.18), solidification speed is taken to be 0.0005, 0.001, 0.0025, or 0.005mm/s. The time grid Δt is 1s.

The solution to the extended model is as follows:

The liquid temperature distribution is calculated by solving the linear system

$$\frac{1}{\alpha_l}\frac{T_l\big|_j^{n+1}-T_l\big|_j^n}{\Delta t} = \frac{1-\theta}{r_j}\frac{1}{\Delta r^2}\left[r_{j+\frac{1}{2}}\left(T_l\big|_{j+1}^{n+1}-T_l\big|_j^{n+1}\right)-r_{j-\frac{1}{2}}\left(T_l\big|_j^{n+1}-T_l\big|_{j-1}^{n+1}\right)\right]$$
$$+\ \frac{\theta}{r_j}\frac{1}{\Delta r^2}\left[r_{j+\frac{1}{2}}\left(T_l\big|_{j+1}^n-T_l\big|_j^n\right)-r_{j-\frac{1}{2}}\left(T_l\big|_j^n-T_l\big|_{j-1}^n\right)\right]\ . \tag{5.22}$$

When the solidification speed is fixed, the wall temperature profile is given by

$$T_0(t) = T_m(t)+\frac{r_0-s(t)}{k_s}\left(-Lu+k_l\frac{T_l\big|_N^{n+1}-T_l\big|_{N+1}^{n+1}}{\Delta r}\right)e^{-\frac{(r_0-s(t))^2}{4\alpha t}}\int_{\frac{r_0-s(t)}{\sqrt{4\alpha t}}}^{\frac{r_0}{\sqrt{4\alpha t}}}\frac{1}{\xi}e^{-\xi^2}d\xi. \tag{5.23}$$

The solid temperature distribution is

$$T_s(r,t) = T_0 - A\int_{\frac{r}{\sqrt{4\alpha t}}}^{\frac{r_0}{\sqrt{4\alpha t}}}\frac{1}{\xi}e^{-\xi^2}d\xi, \tag{5.24}$$

where

$$A = \frac{T_0(t)-T_m(t)}{Integral},\text{ and the } Integral = \int_{\frac{r_0-s(t)}{\sqrt{4\alpha}}}^{\frac{r_0}{\sqrt{4\alpha}}}\frac{1}{\xi}e^{-\xi^2}d\xi.$$

After the wall temperature is held constant, we fix Δs and calculate the time t^{n+1} needed to grow the solid layer by a Δs increment. The next time level is given by

$$t_{i+1} = t_i + \tfrac{1}{6}(k_1+2k_2+2k_3+k_4),\quad i=0,1,2,..,M \text{ with } t^{n+1}=t_M, \tag{5.25}$$

where

$$k_1 = hf(s_i,t_i)$$
$$k_2 = hf(s_i+\tfrac{h}{2},t_i+\tfrac{k_1}{2})$$
$$k_3 = hf(s_i+\tfrac{h}{2},t_i+\tfrac{k_2}{2})$$
$$k_4 = hf(s_i+h,t_i+k_3) \tag{5.26}$$
$$t_0 = t_n,\quad s_0 = s^n$$
$$h = \frac{\Delta s}{M},$$

and

$$f(s,t) = \frac{L}{\dfrac{k_s(T_m(t)-T_0^c)}{(r_0-s(t))\int_{\frac{r_0-s}{\sqrt{4\alpha t}}}^{\frac{r_0}{\sqrt{4\alpha t}}}\frac{1}{x}e^{-x^2}dx}e^{-\frac{(r_0-s)^2}{4\alpha t}}+k_l\dfrac{T_l|_N^n-T_l|_{N+1}^n}{\Delta r}}.$$ (5.27)

The temperature distribution in the solid is

$$T_s(r,t) = T_0 - A\int_{\frac{r}{\sqrt{4\alpha t}}}^{\frac{r_0}{\sqrt{4\alpha t}}}\frac{1}{\xi}e^{-\xi^2}d\xi, \quad where \ A = \frac{T_0(t)-T_m(t)}{\int_{\frac{r_0-s(t)}{\sqrt{4\alpha t}}}^{\frac{r_0}{\sqrt{4\alpha t}}}\frac{1}{\xi}e^{-\xi^2}d\xi}.$$ (5.28)

In Eqs. (5.22)-(5.24), the solidification speed is considered to be 0.0005, 0.001, 0.0025,

or 0.005mm/s. The time grid Δt is 3s, and the space grid Δx is 3E-4mm/s. θ is 0.495.

5.2.3 Calculation of Compound Properties

- Calculation of Eutectic Temperature:

It is noted that ortho-dichlorobenzene and para-dichlorobenzene form a eutectic

solid-liquid phase. The eutectic temperature, T_{eu}, of the system is important because it

provides a constraint in which selective crystallization of a desired component occurs.

Below the eutectic temperature, the binary solution can exist only as a solid. A prediction

of the eutectic temperature, T_{eu}, can be obtained by simultaneously solving for

$X_{liquid}(ortho)$, $X_{liquid}(para)$, and T_m from the Van Laar equation (5.14). This is given by:

$$\ln[X_{liquid}(oDCB)] = \frac{\Delta H_A^f(oDCB)}{R}\left[\frac{1}{T_A^f(oDCB)}-\frac{1}{T_m}\right],$$ (5.29)

and

$$\ln[X_{liquid}(pDCB)] = \frac{\Delta H_A^f(pDCB)}{R}\left[\frac{1}{T_A^f(pDCB)}-\frac{1}{T_m}\right],$$ (5.30)

coupled with the mass balance equation

$$X_{liquid}(oDCB)+X_{liquid}(pDCB) = 1.$$ (5.31)

It should be pointed out that the form of the Van Laar equation used in Eqs. (5.14) and (5.15) assumes that the activity coefficients of both components are equal to one. The assumption that ortho- and para-dichlorobenzene form an ideal mixture was verified by comparing the experimental eutectic temperature reported in the International Critical Tables with the calculated eutectic temperature. Calculated and literature eutectic temperature and concentration varied by only 0.02% and 1%, respectively, demonstrating that ortho- and para-dichlorobenzene can be modeled accurately as an ideal mixture. We found, from the National Institutes of Standards and Technology's pure-component database[75], ΔH_A^f and T_A^f to be 12,930 J/g·mole and 256 K, respectively, for ortho-dichlorobenzene, and 18,160 J/g·mole and 326.1 K, for para-dichlorobenzene. As such, we obtained T_m = 250.2K, which means that T_{eu}=250.2K.

- Calculation of thermal diffusivity

From Chapter 2, we know that thermal diffusivity affects any conductive transient heat transfer process within the medium. It is defined as

$$\alpha = \frac{k}{\rho \cdot C_p},$$
(5.32)

where α is thermal diffusivity (m²/s), k is thermal conductivity (W/(m K)), ρ is density (g/m³),and C_p is specific heat (J/(s K)).

From Eq. (5.32), we can calculate the thermal diffusivity of the solid (pure PDCB), α (in the first model) and α_s (in the second model). Because the liquid represents a mixture of two components, we calculate the compound thermal diffusivity α_l based on the proportion of the two components.

Suppose the compound thermal conductivity, density and specific heat in the liquid are k_l, ρ_l and C_{pl}, respectively, then the compound thermal diffusivity α_l is defined as

$$\alpha_l = \frac{k_l}{\rho_l \cdot C_{pl}}. \tag{5.33}$$

We should point out that as the solidification proceeds, the composition of the components changes with time. Thus, the compound thermal diffusivity changes with time.

- Calculation of L, k_l and ρ_l and C_{pl}

L in the interface Eq. (5.9) for the extended model represents the latent heat per unit volume of the solid. It is calculated by the following formula.

$$L = \rho\lambda', \quad where \ \lambda' = \lambda + C_{pl}(T_l\big|_N^{n+1} - T_m). \tag{5.34}$$

The compound thermal conductivity k_l, density ρ_l, and specific heat c_{pl} in the liquid are used in the extended model to calculate the compound thermal diffusivity. k_l is also used in the interface condition, Eq. (5.9). The values of these parameters change as the solid layer grows and they are directly related to the composition of the two components in the liquid.

The proportion of PDCB in the liquid is given by

$$X_{liquid} = \frac{r_0^2}{[r_0 - s(t)]^2}(X_{init} - X_s) + X_s, \tag{5.35}$$

where X_{init} is the initial proportion of PDCB in the melt, X_s is the proportion of PDCB in the solid, r_0 is the radius of the cylinder, and $s(t)$ is the solid layer width at time t.

Suppose the thermal conductivities, densities, and specific heats of PDCB and ODCB are

k_1, ρ_1, C_{p1}, and k_2, ρ_2, C_{p2}, respectively, then the compound thermal properties will be

$$k_l = X_{liquid}k_1 + (1 - X_{liquid})k_2, \tag{5.36}$$

$$\rho_l = X_{liquid}\rho_1 + (1 - X_{liquid})\rho_2, \tag{5.37}$$

$$C_{pl} = X_{liquid}C_{p1} + (1 - X_{liquid})C_{p2}. \tag{5.38}$$

In this chapter, all the parameters necessary for model application are introduced

and explained. Model results and discussion are given in the next chapter.

CHAPTER SIX

RESULTS AND DISCUSSION

6.1 Simulation Design

In order to test the simplified model in Chapter 3 and the extended model in Chapter 4, we simulate the inward solidification of para-dichlorobenzene from the binary orthochlorobenzen (ODCB) and para-dichlorobenzen (PDCB) compound in a cylindrical crystallizer. The radius of the container is fixed at 60mm.

There are some constraints considered during simulation. First, based on the thermal properties of the two components given in Chapter 5, the eutectic temperature T_{eu} = 250.2K. During solidification, the solid-liquid interface temperature cannot fall below T_{eu}. Second, we set the constraint for the cooling utility to be 290K, which means that when the wall temperature reaches 290K, it will stop decreasing although the solidification will continue for some time. Third, before solidification, we first preheat the melt temperature evenly to a specified temperature. The initial melt temperatures are 316.5K and 324.6K with an initial composition of PDCB of 0.8 and 0.95 mole fractions, respectively. For the simplified model, the melt temperature is maintained constant along the radius. It decreases with the solid-liquid interface temperature and is set to be always 1K higher than the interface temperature. For the extended model, the melt temperature

69

decreases from the center of the cylinder to the solid-liquid interface and is calculated by solving the linear system in Eq. (4.16)-(4.17) as explained in Chapter 4.

To demonstrate the effect of the models, we ran the simulation for different parameters including speed, u (5.0e-6m/s, 2.5e-6/s, 1.0e-6m/s, and 0.5e-6m/s), and initial concentration of PDCB, X_{init} (0.8 and 0.95). In addition to the wall temperature profiles, we also output the interface temperature T_m over time, the solid width s, and the temperature distribution in the solid (simplified model) and in both of the liquid-solid phases (extended model).

6.2 Simulation Results

Figure (6.1) depicts the surface (wall) temperature profiles necessary to achieve four different constant crystallization speeds with an initial para-dichlorobenzene mole fraction of 0.95. The four constant speeds tested were 0.005, 0.0025, 0.001, and 0.0005mm/s. We fixed the wall temperature when it reached the operation limit, that is, $T_0^c = 290$K. The crystallizer wall temperature profiles determined by the models presented in this study represent the temperature profiles that are necessary to maintain a constant crystallization rate. The highest crystallization rate 0.005mm/s required an average wall temperature drop of 64°K/h and 53°K/h for the simplified and the extended model, respectively. A lower cooling rate is not expected to affect product purity, but would increase the cycle time of the process. The increase in the cycle time would increase the size of the static crystallizer necessary to achieve a given throughput. Commercial vendors such as Suzler Chemtech[76] (Switzerland) and BEFS Technologies[77] (France) provide static crystallizers in which the cooling profile is controlled with a high degree of precision. If the standard equipment available from these

or other vendors cannot achieve the desired cooling rate, one would have to determine if the additional capital required to achieve the faster cooling rate outweighed the increase in capital required from a larger crystallizer.
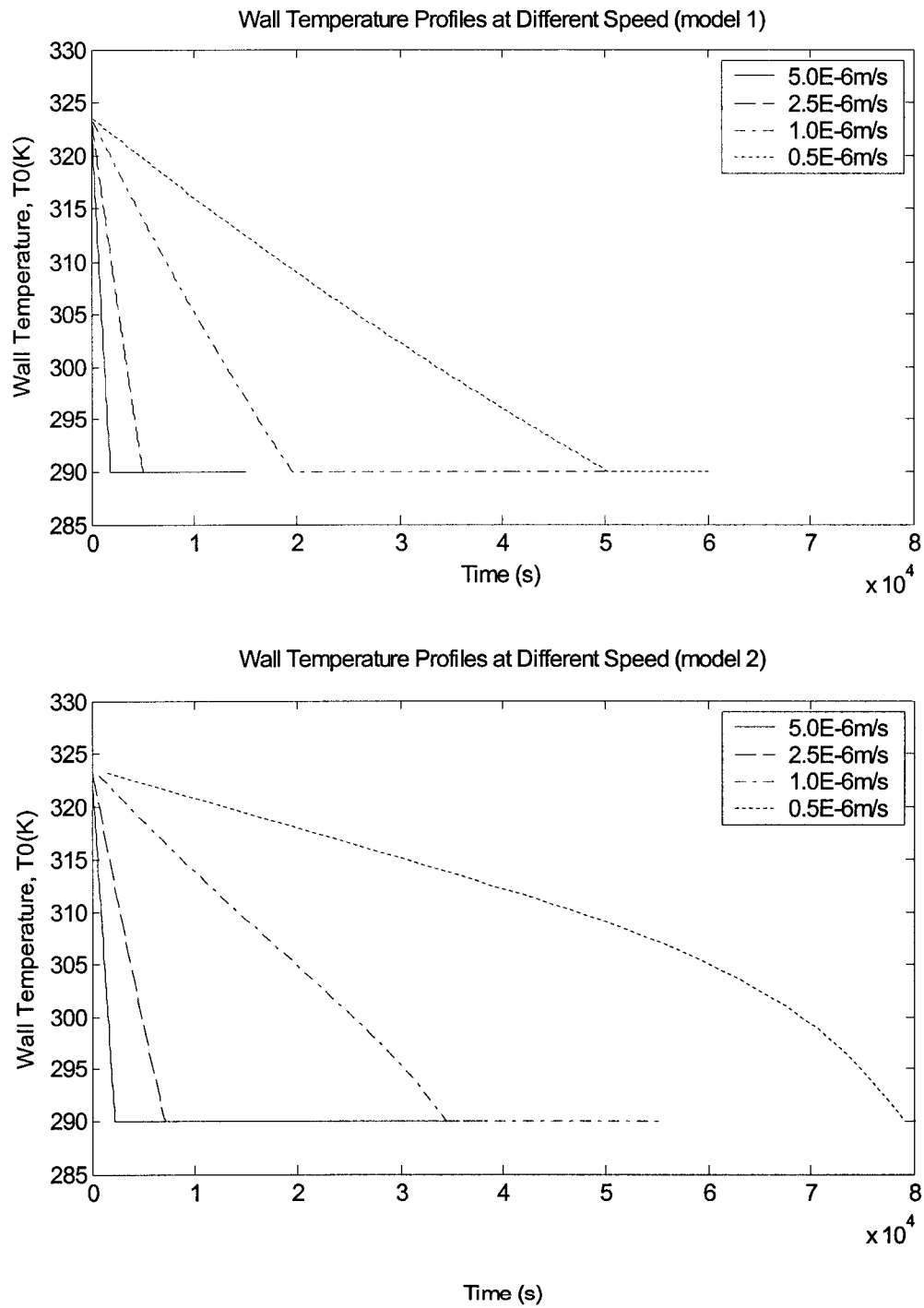
Figure 6.1. Solid-layer growth with $X_{init} = 0.95$ mole fraction at four different constant speeds, 0.005, 0.0025, 0.001, and 0.0005mm/s, and $T_0^c = 290K$

Tables 6.1 and Fig. 6.2 give the statistical results from the two models. From these results we can see that, given a certain constraint T_0^c, one could significantly increase the solid layer growth by decreasing the solidification speed. Also, model 2 (extended model) gives more solid growth than model 1 (simplified model).
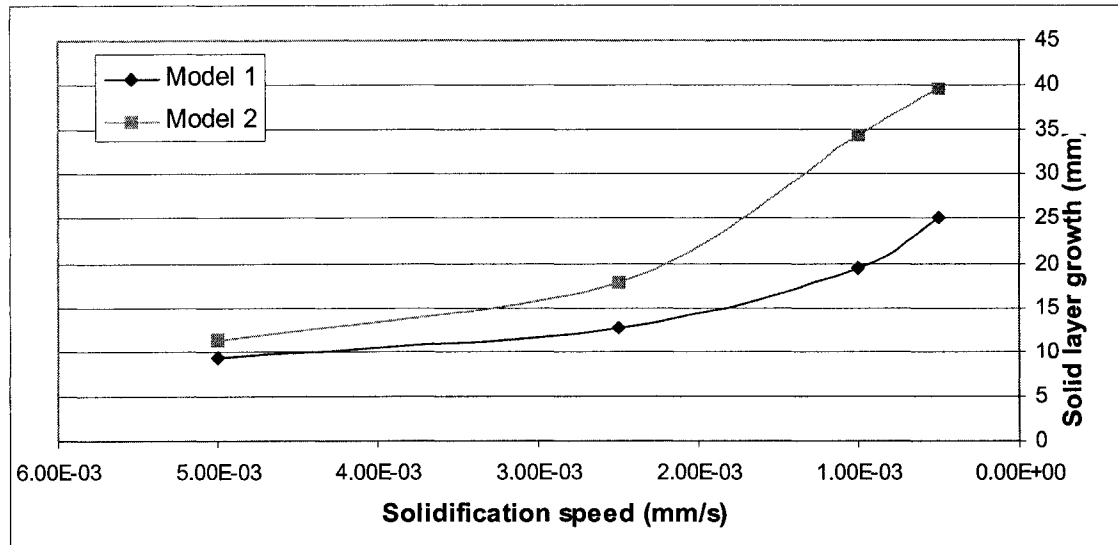
Figure 6.2 Relation of solid layer growth to solidification speed

Table 6.1 Calculation results from the two models at different solidification speeds

	Solidification Speed	Results of Simplified model	Results of Extended model
Decreasing rate of wall temperature	5.0E-6m/s	64K/h	53K/h
	2.5E-6m/s	24K/h	17.1K/h
	1.0E-6m/s	6.2K/h	3.5K/h
	0.5E-6m/s	2.4K/h	1.5K/h
Time to reach the operation limit (290K)	5.0E-6m/s	1,852s	2,238s
	2.5E-6m/s	5,041s	7,134s
	1.0E-6m/s	19,522s	34,380s
	0.5E-6m/s	50,225s	78,990s
Solid layer width when the operation limit is reached	5.0E-6m/s	9.3mm	11.2mm
	2.5E-6m/s	12.6mm	17.8mm
	1.0E-6m/s	19.5mm	34.4mm
	0.5E-6m/s	25.1mm	39.5mm
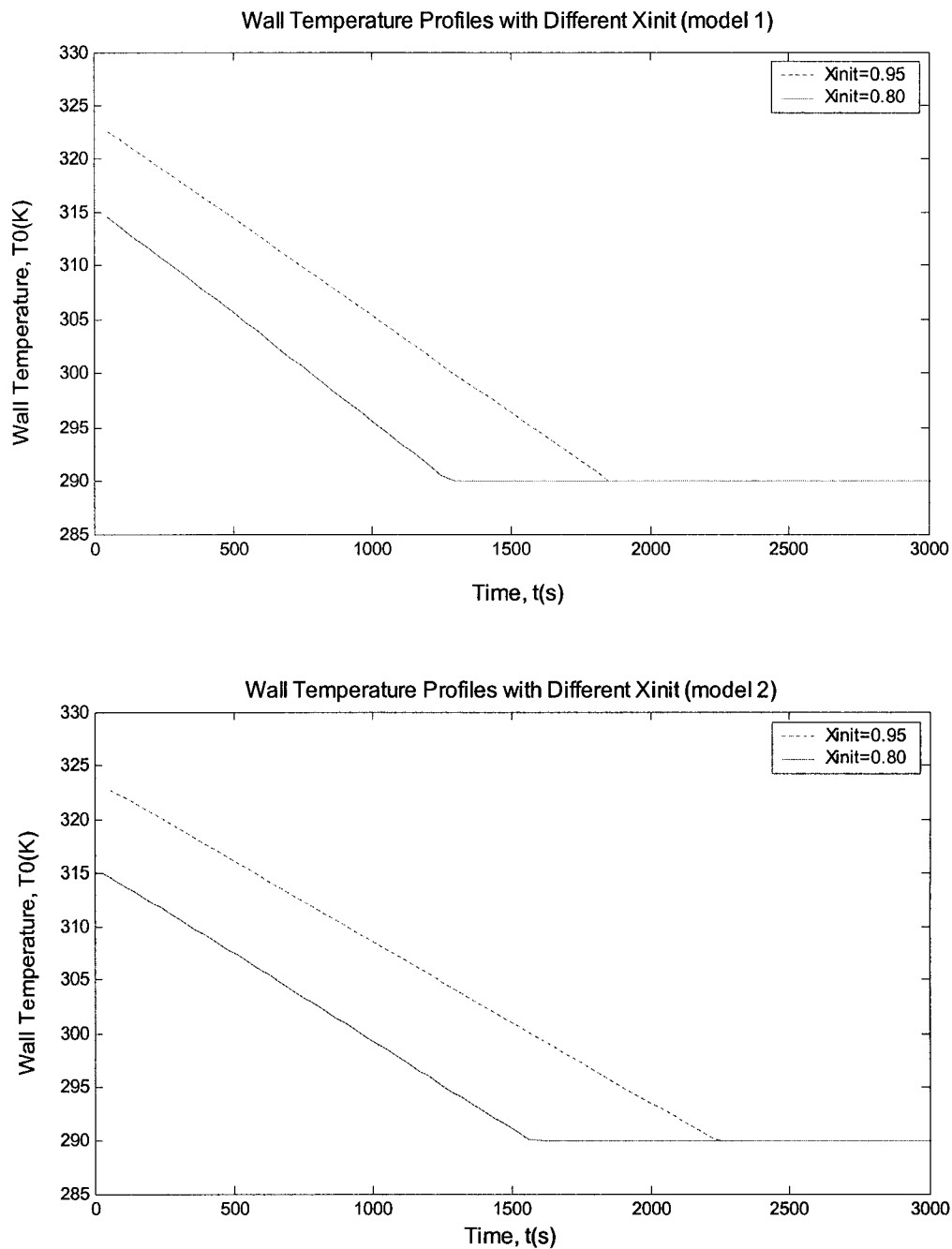
Figure 6.3. Wall temperature profiles over time for two different initial concentrations $X_{init} = 0.95$ and 0.8 with a speed of 0.005mm/s and $T_0{}^c = 290K$

Table 6.2 Results from two models for different initial concentrations

	Initial Concentrations	Simplified Model	Extended Model
Decreasing rate of wall temperature	Xinit = 0.95	64K/h	53K/h
	Xinit = 0.8	72K/h	59K/h
Time to reach the operation limit of 290K	Xinit = 0.95	1,852s	2,238s
	Xinit = 0.8	1,276s	1,569s
Solid layer width when the operation limit is reached	Xinit = 0.95	9.3mm	11.2mm
	Xinit = 0.8	6.4mm	7.8mm

Figure 6.3 and Table 6.2 show the crystallizer wall temperature over time for two different initial concentrations, X_{init} = 0.95 and 0.80. The crystallization rate for both concentrations is maintained at a constant rate of 0.005mm/s. The models predict that the lower initial concentration will require a slightly higher average rate of decrease in crystallizer wall temperature to maintain the same crystallization rate, and the lower initial concentration will also grow less solid when the operation limit is reached. Both models show the same trends, and the extended model, compared with the simplified model, requires less rate of decrease in crystallizer wall temperature, needs more time to reach the operation limit, and can grow more solid.
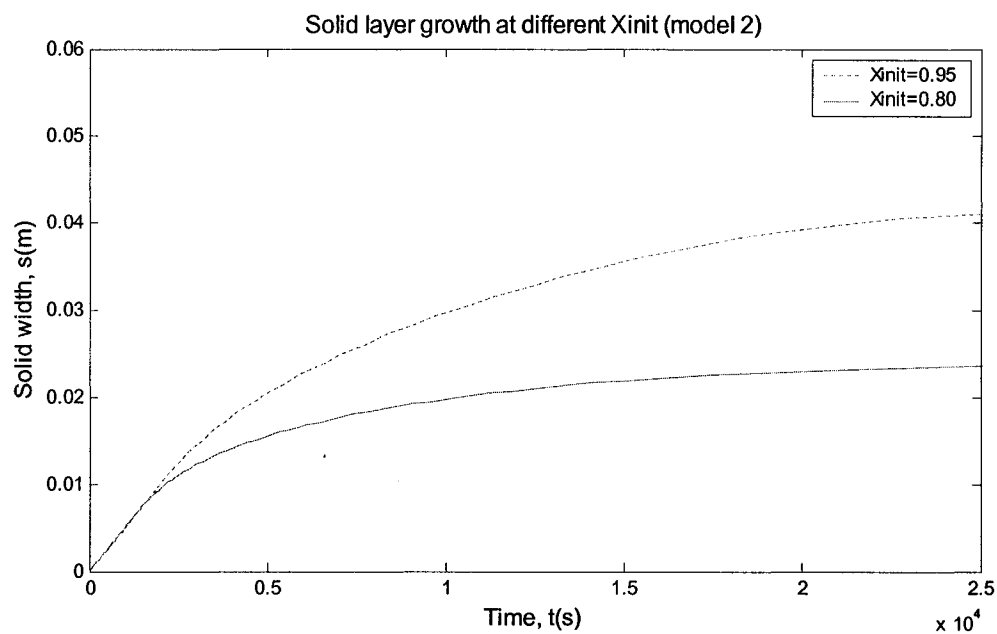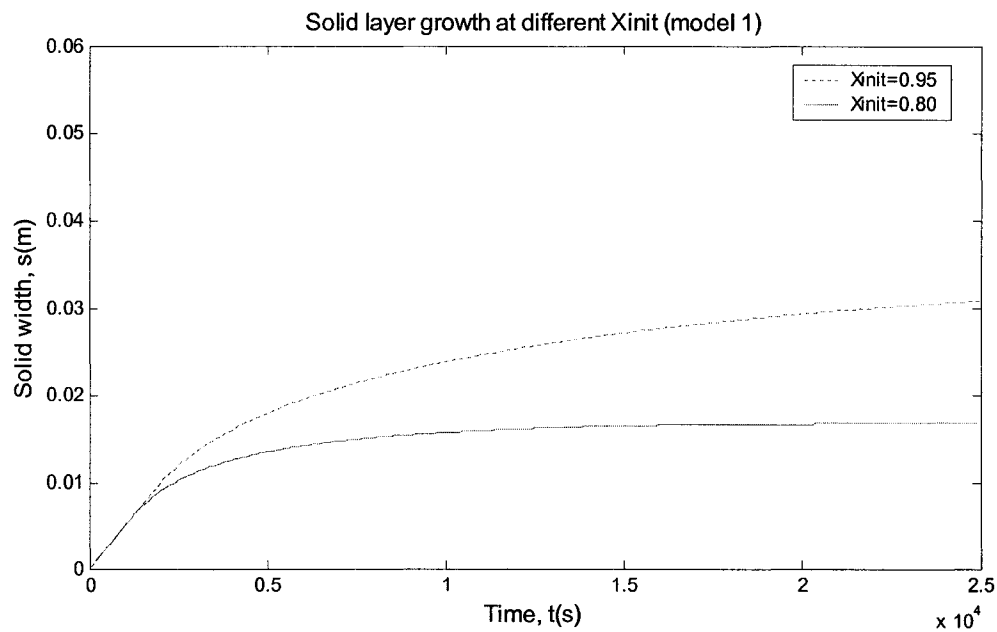
Figure 6.4. Total solid-layer growth from melt crystallization
with a speed of 0.005mm/s and $T_0^c = 290K$

Fig. 6.4 shows solidification in the radial direction that occurs given the cooling rate of 0.005mm/s and T_0^c = 290K. The position depicted in Fig. 6.4 is the interface between the solid and liquid at a given time. Because the lower concentration requires a higher rate of decrease in the crystallizer wall temperature in order to achieve a given solidification speed, it also needs less time to reach the operation limit (in this case, 290K), as shown in Table 6.2. After the wall temperature is fixed at 290K, the solidification speed slows down. As time proceeds, the solid layer growth becomes slower and slower. If a threshold for the growth speed of the solid is specified, one can use the model to calculate the time required for the solidification speed to fall below the threshold, thus leading for a termination for the crystallization process.

Fig. 6.4 also indicates that a lower initial concentration will grow less solid after the wall temperature is fixed.
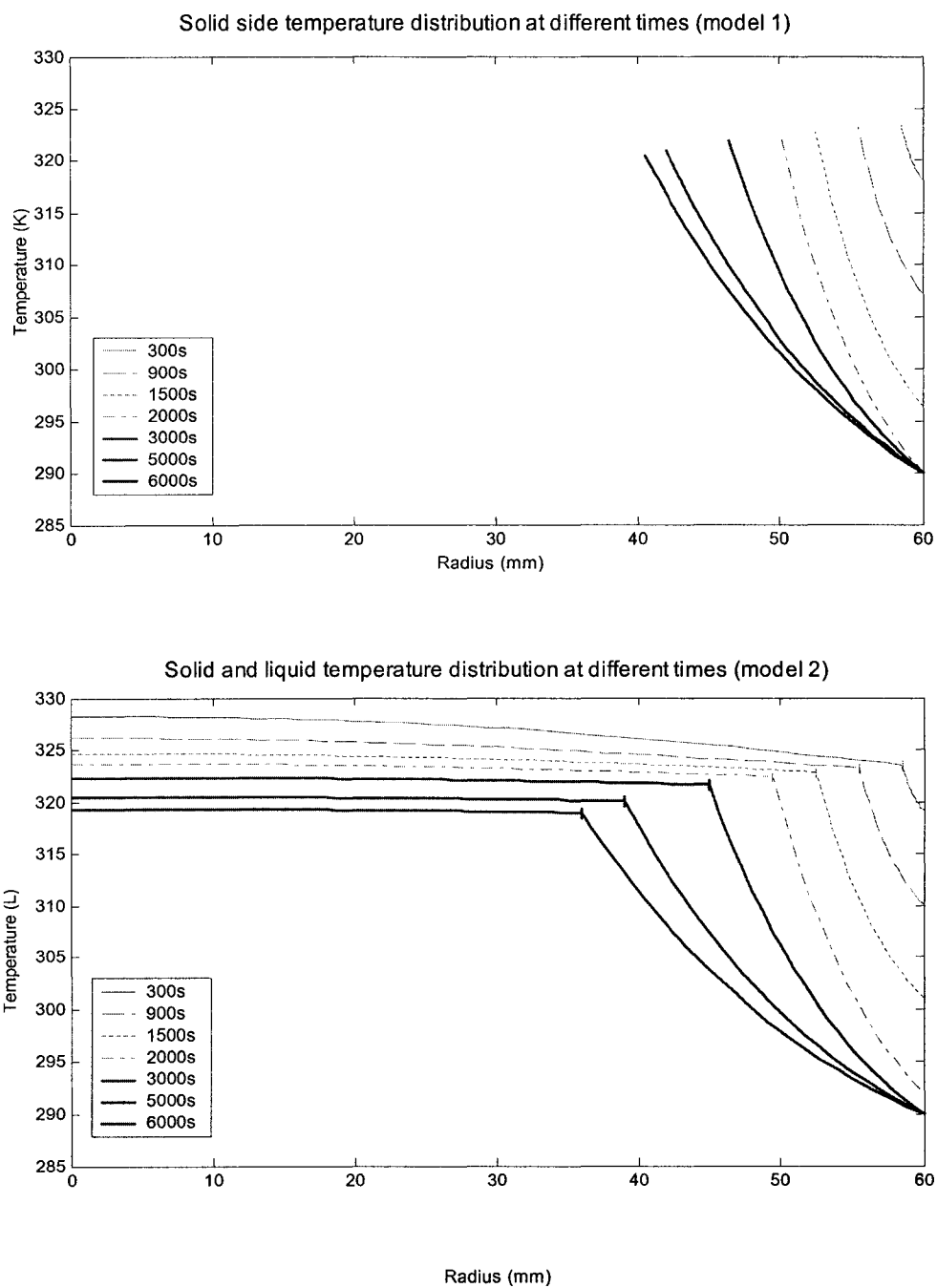
Figure 6.5. Temperature distributions at different times

Figure 6.5 depicts the temperature profiles that exist in the solid phase (simplified model) and both solid and liquid phases (extended model) for $X_{init} = 0.95$ at different times. The solid-liquid interface for the extended model is identified by a small vertical bar in the figure. The crystallization rate was held constant at 0.005mm/s. Large temperature gradients are clearly evident in the solid phase. Since the liquid has a lower compound thermal conductivity than the solid (see Chapter 5 for parameters), it shows lower temperature gradients. The poor thermal conductivity of the organic compounds creates challenges in maintaining the desired crystallization rate.
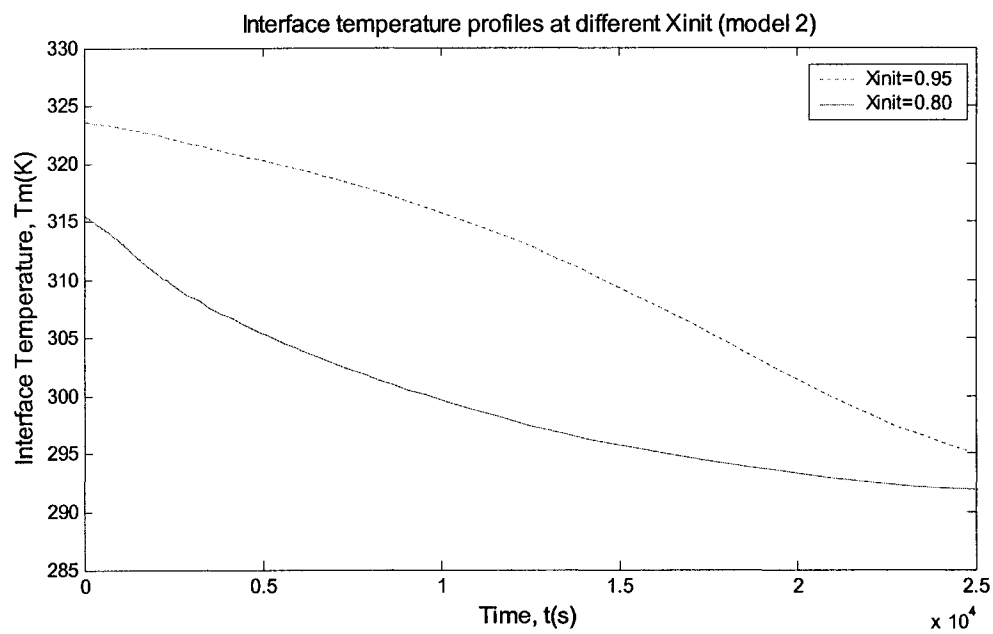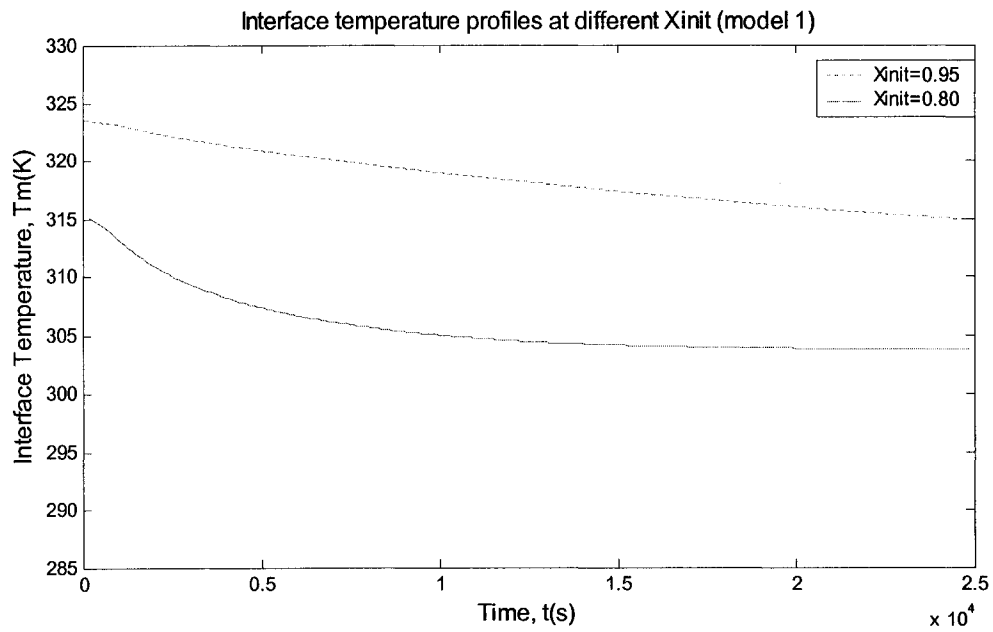
Figure 6.6. Interfacial temperature change with time

Figure 6.6 shows the solid/liquid interface temperatures as a function of time for X_{init} = 0.95 and 0.80. The reduction in interfacial temperature is determined by the liquid concentration using the Schröder-van Laar equation. The reduction in the melting point as a function of bulk liquid concentration must be accounted for, due to the significant thermal resistant that the solid layer imposes. Neglecting the change in liquid composition would predict a shorter cycle time than required, which would result in undersizing of the crystallizer equipment.

6.3 Discussion

For the simplified model (model 1), the liquid is fully stirred and the temperature in the liquid is constant in the radial direction. Heat convection is considered in the model. For the extended model (model 2), the liquid is still and the liquid's temperatures decrease from the center of the cylinder to the solid-liquid interface. Based on these facts, the two models adopted different interface equations. From the results, we can see that by changing the solidification speed from 0.5e-6m/s to 2.5e-6m/s, the cooling rates of the crystallizer wall fall between 2.4~24K/h and 1.5~17.1K/h for the simplified and extended model, respectively. These are in accordance with the experimental results by Duardani, et al[78]. Guardani, et al, chose cooling rates ranging from 2.4K/h to 24K/h for crystallizing e-caprolactam from a binary compound with water as impurity. They also considered two cases, static layer crystallization, in which only natural convection influences mass and heat transfer, and dynamic layer crystallization, in which forced convection is obtained by pumping the mother liquor as a falling film on a heat exchanger.

From the results of this study, we can conclude that the simplified model needs higher cooling rate than the extended model to achieve the same solid layer growth rate. In other words, higher layer growth rate can be obtained when using the extended model at the same cooling rate. This is due to the heat transfer conditions between the melt and the solid-liquid interface. Since, in the extended model, the melt is still and a temperature profile across the melt is established, the melt can reach a lower temperature during the crystallization time.

Results from the two models show the same trend, namely that a lower initial concentration requires a higher cooling rate of the crystallizer wall in order to maintain the same crystallization rate. Hence, less time is needed to reach the operation constraint, thus leading to less solid layer growth.

The extended model is preferred, since more crystal growth will occur under the same conditions as for the simplified model. A combination of the extended model with information concerning investment and operating costs for items such as the heat exchange area, pumping, and heating power, will lead to an optimal design of a layer crystallization process.

CHAPTER SEVEN

SUMMARY AND FUTURE WORK

7.1 Summary

In this dissertation we combine analytic and numerical methods for predicting solid-layer growth from melt crystallization. First, we predict the wall temperature profile over time for achieving solid separation from the melt at a constant rate. Second, we predict the rate of crystallization (or solid formation) when the wall temperature is held constant at a certain value equal to the lowest temperature that is operationally feasible. Third, we predict the temperature distribution in each of the solid and liquid phases. By considering a temperature distribution in the solid phase and holding the liquid phase's temperature constant in the radial direction, an analytic model was developed by using dimensional analysis. This model was then extended numerically to account for a temperature distribution in each of the phases, liquid and solid. Applications of the two models were demonstrated with an example involving crystallization of para-dichlorobenzene from the ortho-dichlorobenzene and para-dichlorobenzene binary melt. Results from both models were analyzed and compared.

Results showed that a lower initial concentration required a higher cooling rate of the crystallizer wall in order to maintain the same crystallization rate. Hence, less time was needed to reach the wall temperature operation constraint, thus leading to less solid

Reproduced with permission of the copyright owner. Further reproduction prohibited without permission.

layer growth. By comparing the results of the two models, one can conclude that the second model in which there is a melt temperature gradient in the radial direction is preferred, since more crystal growth will occur under the same conditions as for the first model.

7.2 Future Work

Future studies to consider are the following:

- In the first model (analytic model), the temperature in the melt is considered constant in the radial direction. During modeling, the melt temperature is set to be a constant degree higher than the solid-liquid interface temperature. Other cases may be considered such as a melt temperature which decreases at a different rate from the solid-liquid interface temperature, or a melt temperature that is held constant over time.

- There are three modes of directional melt crystallization as explained in Chapter 2. This study deals with the inward cylindrical radial mode. The models built here can be easily modified to adapt the outward cylindrical radial mode.

- The examples chosen in this study are two organics, para-dichlorobenzen and ortho-dichlorobenzen. Further studies may consider different organics, or non-organic substances.

- For model validation, experiments can be run with the same wall temperature profile (cooling rate) as predicted from each model, and observed solid layer growth can be compared to that predicted from the model.

APPENDIX

SOURCE CODE

84

Program 1: Source code for simplified model

```
/********************************************************************
This program uses simplified model to calculate solid layer growth at constant speed. The
liquid temperature is considered constant in radial direction. First, it calculates the
crystallizer wall temperature profile at a given constant solidification speed. Then when
the wall temperature reaches the operation limit (290K), the solid layer growth rate is
calculated. The temperature distributions of solid in both cases are calculated.
********************************************************************/
#include <iostream.h>
#include <math.h>


double C;            //the solidification speed
double r0;           //the radius of the cylinder
double T0;           //the outer wall temperature
double Tb;           //the bulk(liquid) temperature
double Tm;           //the solid-liquid interface temperature
double Teu;          //Eutectic temperature for the binary mixture

double lamda2;       //sum of heat of crystallization and latent heat

//constant variables
double alfa;         //thermal diffusivity of solid (PDCB)
double Ks;           //thermal conductivity of solid
double P;            //density of solid
double lamda;        //heat released by crystallization
double he;           //heat convection coefficient
double Cpl;          //specific heat
double Xliquid;      //composition of PDCB in liquid
double deltaHaf;     //molar heat of fusion
double Taf;          //liquidus temperature of PDCB
double Xinit;        //initial composition of PDCB in liquid
double Xs;           //mole function params.
double R=8.32/147;   //gas constant

const int DIFF = 1;        // Tb - Tm

//constant for controling the output
const int OUT_Tm = 1;
const int OUT_T0 = 2;
const int OUT_Ts = 3;

const int OUT = OUT_T0;

//=================================================================
// function used to calculate the term inside the integration
// input:  x
// output: value of the term
//=================================================================
double fun(double x)
{
        return 1/x * exp(-x*x);
}
```

```
//========================================================
// function used to calculate interface temperature
// input:  solid layer width ss
// output: interface temperature Tm
//========================================================
double getTm(double ss)
{

        return 1.0 / ( 1.0/Taf - (R/deltaHaf)*log( r0*r0/((r0-ss)*(r0-ss)) *(Xinit-Xs)+Xs) );

}


//========================================================
// function used to calculate integaration
// input:  lower limit and upper limit
// output: rerult of integration
//========================================================
double myIntegral(double bot, double top)
{

        long int n = 10000;
        double h = (top - bot)/n;
        double XI, XI0, XI1, XI2, X;

        XI0 = fun(bot) + fun(top);
        XI1 = 0;
        XI2 = 0;

        for(int i= 1; i<n; i++)
        {
                X = bot + i*h;

                if(i%2==0)
                        XI2 = XI2 + fun(X);
                else
                        XI1 = XI1 + fun(X);
        }

        XI = h*(XI0 + 2*XI2 + 4*XI1)/3;
        return XI;

}


//========================================================
// function for calculation the solid width after stopping
// decreasing of T0, using Runge-Kutta iteration.
//--------------------------------------------------
double function(double t, double s)
{

        double bot, top, integral, result;

        top = r0/sqrt(4*alfa*t);
        bot = (r0-s)/sqrt(4*alfa*t);


        integral = myIntegral(bot, top);
```

Tm = 1.0 / (1.0/Taf - (R/deltaHaf)*log(r0*r0/((r0-s)*(r0-s)) *(Xinit-Xs)+Xs));

Tb = Tm + DIFF; //temporarily set Tb-Tm constant

lamda2 = lamda + Cpl * (Tb - Tm);

result = ((Tm - T0)*Ks/(r0-s) * exp((-1)*(r0-s)*(r0-s)/(4*alfa*t)) / integral - he*(Tb-Tm)) / (P*lamda2);

```
        return result;

}

double RungeKutta(double a, double b, double init)
{
        double w;
        double k1, k2, k3, k4;
        const int N = 10;
        double h, t;

        h = (b-a)/N;
        t = a;
        w = init;

        for(int i=1;i<=N;i++)
        {
                k1 = h*function(t, w);
                k2 = h*function(t + h/2, w + k1/2);
                k3 = h*function(t + h/2, w + k2/2);
                k4 = h*function(t + h, w + k3);

                w = w + (k1 + 2*k2 + 2*k3 + k4) / 6;
                t = a + i*h;
        }

        return w;

}

double Euler(double a, double b, double init)
{
        double dt;
        double ret;

        dt = b - a;
        ret = init + dt * function(a, init);

        return ret;
}

//===============================================
// beginning of the main function
//===============================================
int main(void)
{
```

```
double s;
double bot, top, integral;
double A, Ts, r;
int t, N;

//initialize the parameters
r0              = 0.060;         // m - the radius of the bolk melt
s               = 0;

//thermal properties of solid (pure PDCB)
Ks              = 0.14473;       // W/(m k)
Cpl             = 1.005;         // J/gK
P               = 1.241e6;       // g/m3
alfa    = Ks/(P*Cpl);            // =1.1604E-7

lamda   = 18160/147;    // J/g
he              = 150;  // W/mK

deltaHaf= 18160/147;    // J/gmole
Taf             = 326.1; // K
Xs              = 1.0;

//=====variables================================================
Xinit   = 0.95;
C       = 5e-6;
//=============================================================

Teu     = 250.2;        //K eutectic temperature

//print out the titles in the output
cout<<"%=================================================="<<endl;
cout<<"%== C="<<C<<" -- Xinit="<<Xinit<<endl;
switch(OUT)
{
case OUT_T0:
case OUT_Tm:
        cout<<"%t \t s \t Tm \t T0";
        break;

case OUT_Ts:
        cout<<"%r \t T";
        break;

}
cout<<endl;

//constant solidification speed
for(t=1;t<=70000;t++)
{
        s = C*t;
        Tm = getTm(s);

        Tb = Tm + DIFF;

        lamda2 = lamda + Cpl * (Tb - Tm);
```

```
top = r0/sqrt(4*alfa*t);
bot = (r0-s)/sqrt(4*alfa*t);

integral = myIntegral(bot, top);

if(integral==0)
        T0 = Tm;
else
        T0 = Tm - 1.0/Ks *( P*lamda2*C + he*(Tb-Tm) )*(r0-s) * exp((r0-s)*(r0-
s)/(4*alfa*t)) * integral;


switch(OUT){
case OUT_T0:
case OUT_Tm:
        if(t%200==0)
                cout<<t<<"\t"<<s<<"\t"<<Tm<<"\t"<<T0<<endl;
        break;
case OUT_Ts:
        //output the inner temperatures in the solid
        if(t%300 == 0)
        {
                A = (T0-Tm) / integral;

                cout<<"%=======================================\n";
                cout<<"%s:"<<s<<" t:"<<t<<" Tm:"<<Tm<<" T0:"<<T0<<endl;

                top = r0/sqrt(4*alfa*t);
                for(int i=0;i<=20;i++)
                {
                        r = r0 - i*(s/20);
                        bot = r / sqrt(4*alfa*t);
                        Ts = T0 - A * myIntegral(bot, top);
                        cout<<r*1000<<"\t"<<Ts<<endl;
                }
        }
        break;
}


//check if the solidification ends
if(Tm<=Teu){
        //print out the ending temperature
        cout<<"\n Solidification stopped.\n";
        cout<<"% t = "<<t <<"\tT0 = "<<T0<<"\ts = "<<s<<"\tTm = "<<Tm;
        return 0;
}

if(T0<=290){ // ***********continue calculation by fixing T0
        cout<<"% t = "<<t <<"\tT0 = "<<T0<<"\ts = "<<s<<"\tTm = "<<Tm;
        cout<<"\n%===========Fixing T0=======";
        break;
}

}
```

```
cout<<endl<<"%Stop decreasing T0."<<endl;

//calculate the solid growth after stopping decreasing T0
N = t-1;

double a, b, init, dR;

for(t=N+1;t<=60000;t++)
{

        a = t-1;
        b = t;
        init = s;

        dR = RungeKutta(a, b, init) - s;
        //s = Euler(a, b, init);        //updating s and Tm
        s = s + dR;

        Tm = 1.0 / ( 1.0/Taf - (R/deltaHaf)*log( r0*r0/((r0-s)*(r0-s)) *(Xinit-Xs)+Xs) );

        Tb = Tm + DIFF;


        switch(OUT)
        {
        case OUT_T0:
        case OUT_Tm:
                if(t%100==0)
                        cout<<t<<"\t"<<s<<"\t"<<Tm<<"\t"<<T0<<"\t% "<<dR<<endl;
                break;

        case OUT_Ts:
                if(t%1000 == 0)
                {
                        top = r0/sqrt(4*alfa*t);
                        bot = (r0-s)/sqrt(4*alfa*t);

                        integral = myIntegral(bot, top);

                        A = (T0-Tm) / integral;


                        cout<<"%=================================================\n";
                        cout<<"%s:"<<s<<" t:"<<t<<" Tm:"<<Tm<<" T0:"<<T0<<"
deltaR:"<<dR<<endl;

                        top = r0/sqrt(4*alfa*t);
                        for(int i=0;i<=20;i++)
                        {
                                r = r0 - i*(s/20);
                                bot = r / sqrt(4*alfa*t);
                                Ts = T0 - A * myIntegral(bot, top);
                                cout<<r*1000<<"\t"<<Ts<<endl;
                        }
                }
                break;
```

```
                    }

        } //end of calculation after stopping T0

        return(0);
}
```

Program 2: Source code for extended model

```
/****************************************************************
This program uses extended model to calculate solid layer growth at constant speed. Both
solid and liquid phases have temperature gradients in radial direction. First, it calculates
the crystallizer wall temperature profile at a given constant solidification speed. Then
when the wall temperature reaches the operation limit (290K), the solid layer growth rate
is calculated. The temperature distributions of solid and liquid in both cases are
calculated.
****************************************************************/
#include <iostream.h>
#include <math.h>

double C;          //the solidification speed
double r0;         //the radius of the cylinder
double T0;         //the outer temperature
double Tb;         //the bulk(liquid) temperature
double Tm;         //the solid-liquid interface temperature
double Teu;        //Eutectic temperature for the binary mixture

double alfa;       //heat diffusivity of solid
double alfa2;      //heat diffusivity of liquid (compound)
double s;          //solid layer width
double r;          //radius variable
double rl;         //index of left grid point
double rr;         //index of right grid point
double Ks;         //thermal conductivity of solid
double Km;         //thermal conductivity of liquid (compound)
double P;          //density of solid
double Pl;         //density of liquid (compound)
double lamda;      //heat released from crystallization
double lamda2;     //sum of heat released from crystallization and sensible heat
double Cpl;        //specific heat
double L;          //latent heat for unit volume of phase transision

double Xliquid;    //Composition of PCB in the liquid
double deltaHaf;   //molar heat of fusion
double Taf;        //
double Xinit;      //initial composition of PCB in the liquid
double Xs;         //composition of PCB in the solid
double R = 8.32/147;   //gas constant. J/gmold K

double theta = 0.495;   //distribution factor for implicit method

double deltaR;     //grid size
double deltaT;     //time step
double deltaBigR;  //space step

long int Jinit;    //number of grid points per space step (deltaBigR)
long int I;        //number of grid points in liquid phase
long int J;        //number of grid points in solid phase

//constant for controling the output
```

```
const int OUT_Tm = 1;
const int OUT_T0 = 2;
const int OUT_Ts = 3;

const int OUT = OUT_T0;

//variables for calculation temperature distributions
const int MAX_GRID = 200000;    //total number of grid points through solid and liquid
const double PAI = 3.14159265;
double *T;          //temprature distributions
double *Tarray;   //the linear system for solving liquid temperature distribution for each step

//variables initializing linear system of the implicit scheme
double t0, t1, t2, t3, t4, t5;

double W;          //Walts

int i, j, k;
int pre =0, cur =1;          //variables for tracking iterations
int step1, step2;             //variables for formating the output

//function declarisions
void getTb();
double getAlfa2();
void UpdateKmP(double ss);

//function for calculation interface temperature
double getTm(double ss)
{
        return 1.0 / ( 1.0/Taf - (R/deltaHaf)*log( r0*r0/((r0-ss)*(r0-ss)) *(Xinit-Xs)+Xs) );
}

//function for calculation the term inside integration
double fun(double x)
{
        return 1/x * exp(-x*x);
}

//function to calculate the integration
double myIntegral(double bot, double top)
{

        long int n = 10000;
        double h = (top - bot)/n;
        double XI, XI0, XI1, XI2, X;

        XI0 = fun(bot) + fun(top);
        XI1 = 0;
        XI2 = 0;

        for(int i= 1; i<n; i++)
        {
                X = bot + i*h;

                if(i%2==0)
```

```
                              XI2 = XI2 + fun(X);
                 else
                              XI1 = XI1 + fun(X);
          }

          XI = h*(XI0 + 2*XI2 + 4*XI1)/3;
          return XI;
}
```

```
//=======================================================
// function for calculation the solid width after stopping
// decreasing of T0, using Runge-Kutta iteration.
//-------------------------------------------------
double function(double tt, double ss)
{

          double bot, top, integral, result;

          top = r0/sqrt(4*alfa*tt);
          bot = (r0-ss)/sqrt(4*alfa*tt);


          integral = myIntegral(bot, top);

          result = ( (Tm - T0)*Ks/(r0-ss) * exp((-1)*(r0-ss)*(r0-ss)/(4*alfa*tt)) / integral - Km*(Tb-
Tm)/deltaR ) / L;

          return result;

}
```

```
//=======================================================
// function for calculation the next time level after stopping
// decreasing of T0, using Runge-Kutta iteration.
//-------------------------------------------------
double function2(double ss, double tt)
{

          double bot, top, integral, result;

          top = r0/sqrt(4*alfa*tt);
          bot = (r0-ss)/sqrt(4*alfa*tt);


          integral = myIntegral(bot, top);

          result = ( (Tm - T0)*Ks/(r0-ss) * exp((-1)*(r0-ss)*(r0-ss)/(4*alfa*tt)) / integral + Km*(Tb-
Tm)/deltaR ) / L;

          return 1/result;

}

double RungeKutta(double sa, double sb, double t0)
{
```

```
        double w;
        double k1, k2, k3, k4;
        const int N = 10;
        double h, s0;

        h = (sb-sa)/N;
        s0 = sa;
        w = t0;

        for(int i=1;i<=N;i++)
        {
                k1 = h*function2(s0, w);
                k2 = h*function2(s0 + h/2, w + k1/2);
                k3 = h*function2(s0 + h/2, w + k2/2);
                k4 = h*function2(s0 + h, w + k3);

                w = w + (k1 + 2*k2 + 2*k3 + k4) / 6;
                s0 = s0 + i*h;
        }

        return w;

}


double Euler(double a, double b, double init)
{
        double dt;
        double ret;

        dt = b - a;
        ret = init + dt * function(a, init);

        return ret;
}

//start of the program
int main(void)
{
        double s;
        double bot, top, integral;
        double A, Ts, r, t;
        int N;

        //initialize the parameters
        r0              = 0.060;        // m - the radius of the bolk melt
        s               = 0;

        //thermal properties of solid (pure PDCB)
        Ks              = 0.14473;      // W/(m k)
        Cpl             = 1.005;        // J/gK
        P               = 1.241e6;      // g/m3
        alfa    = Ks/(P*Cpl);   // =1.1604E-7

        lamda   = 18160/147;    // J/g

        deltaHaf= 18160/147;    // J/gmole
```

```
Taf             = 326.1;          // K
Xs              = 1.0;

//====variables=======================================================
Xinit    = 0.95;
C        = 5e-6;
//====================================================================

Teu      = 250.2;          //eutectic temperature

T        = new double[(MAX_GRID+1)*2*sizeof(double)];
Tarray   = new double[(MAX_GRID+1)*4*sizeof(double)];
Jinit    = 50;
N        = 0;

deltaR    = r0 / MAX_GRID;
deltaBigR = deltaR * Jinit;
deltaT    = deltaBigR / C;

I = MAX_GRID -1;          //grid size in the melt
J = 0;                    //grid size in the solid

pre = (N+1) % 2;
cur = N % 2;

//initialize bulk temperature Tb
Xliquid = Xinit;   //first value = Xinit
Tm = (Taf * deltaHaf) / (deltaHaf - Taf * R * log(Xliquid));

for(i = 0; i<MAX_GRID; i++)
            T[cur*MAX_GRID + i] = Tm + 5;


//====================================================================
//print out the titles in the output
cout<<"%=============================================================="<<endl;
cout<<"%== C="<<C<<" -- Xinit="<<Xinit<<" -- dT="<<deltaT<<endl;
switch(OUT)
{
case OUT_T0:
case OUT_Tm:
        cout<<"%t \t s \t Tm \t T0";
        break;

case OUT_Ts:
        cout<<"%r \t T";
        break;

}
cout<<endl;


for(i=1;i<=70000;i++)
{
        //increment the width
        N++;
        t = deltaT * N;
```

```
J += Jinit;
I -= Jinit;

//get new solid thickness
s = C*t;

//set the pointer of the old T and new T
pre = (N+1) % 2;
cur = N % 2;

//calculate new inner boundary condition
Tm = getTm(s);

//calculate the liquid temperature distribution
getTb();

//calculate the compound properties
UpdateKmP(s);

//calculate the wall temperature
top = r0/sqrt(4*alfa*t);
bot = (r0-s)/sqrt(4*alfa*t);
integral = myIntegral(bot, top);

lamda2 = lamda + Cpl * (Tb - Tm);
L = P*lamda2;

if(integral==0)
        T0 = Tm;
else
{
        double tmp = exp((r0-s)*(r0-s)/(4*alfa*t));
        T0 = Tm + (r0-s)/Ks * (-L*C + Km*(Tb-Tm)/deltaR) * integral * exp((r0-
s)*(r0-s)/(4*alfa*t));
}

switch(OUT){
case OUT_T0:
case OUT_Tm:
        if(i%10==0)
                cout<<t<<"\t"<<s<<"\t"<<Tm<<"\t"<<T0<<endl;
        break;
case OUT_Ts:
        //output the inner temperatures in the solid and liquid phases
        if(i%100 == 0)
        {
                if(I>50)
                        step1 = I/50;
                else
                        step1 = 1;
                if(J>50)
                        step2 = J/50;
                else
                        step2 = 1;
```

```
cout<<"%=======================================\n";
cout<<"%s:"<<s<<" t:"<<t<<" Tm:"<<Tm<<" T0:"<<T0<<endl;

//liquid side temperature distribution
for(k=0;k<I;k+=step1)
        cout<<k*deltaR*1000<<"\t"<<T[cur*MAX_GRID+k]<<endl;

//interface temperature
//output a vertical bar to mark the interface
for(k=0;k<10;k++)
        cout<<I*deltaR*1000<<"\t"<<Tm-0.5+k/10.0<<"\t%-----
"<<endl;

//solid side temperature distribution
A = (T0-Tm) / integral;

top = r0/sqrt(4*alfa*t);
for(k=20;k>=0;k--)
{
        r = r0 - k*(s/20);
        bot = r / sqrt(4*alfa*t);
        Ts = T0 - A * myIntegral(bot, top);
        cout<<r*1000<<"\t"<<Ts<<endl;
}
}
break;
}


//check if the solidification ends
if(Tm<=Teu){
        //print out the ending temperature
        cout<<"\n% Solidification stopped.\n";
        return 0;
}

if(T0<=290){ // ***********continue calculation by fixing T0
        cout<<"% t = "<<t <<"\tT0 = "<<T0<<"\ts = "<<s<<"\tTm = "<<Tm;
        cout<<"\n% ============Fixing T0=======";
        break;
}
}

cout<<endl<<"%==Stop decreasing T0."<<endl;

//calculate the solid growth after stopping decreasing T0
for(j=i;j<=15000;j++)
{
        N++;
        s = s + deltaBigR;
        J += Jinit;
        I -= Jinit;

        deltaT = RungeKutta(s-deltaBigR, s,t) - t;
```

```
t = t + deltaT;

//set the pointer of the old T and new T
pre = (N+1) % 2;
cur = N % 2;

Tm = getTm(s);
getTb();

UpdateKmP(s);

top = r0/sqrt(4*alfa*t);
bot = (r0-s)/sqrt(4*alfa*t);
integral = myIntegral(bot, top);

lamda2 = lamda + Cpl * (Tb - Tm);
L = P*lamda2;

switch(OUT)
{
case OUT_T0:
case OUT_Tm:
        if(j%20==0)
                cout<<t<<"\t"<<s<<"\t"<<Tm<<"\t"<<T0<<"\t% "<<deltaT<<endl;
        break;

case OUT_Ts:
        if(j%200 == 0)
        {

                if(I>50)
                        step1 = I/50;
                else
                                step1 = 1;
                if(J>50)
                                step2 = J/50;
                else
                                step2 = 1;


                cout<<"%============================================\n";
                cout<<"%s:"<<s<<" t:"<<t<<" Tm:"<<Tm<<" T0:"<<T0<<"
deltaT:"<<deltaT<<endl;

                //liquid side temperature distribution
                for(k=0;k<I;k+=step1)
                        cout<<k*deltaR*1000<<"\t"<<T[cur*MAX_GRID+k]<<endl;

                //interface temperature
                for(k=0;k<10;k++)
                        cout<<I*deltaR*1000<<"\t"<<Tm-0.5+k/10.0<<"\t%-----
"<<endl;

                //solid side temperature distribution
                A = (T0-Tm) / integral;
```

```
                        top = r0/sqrt(4*alfa*t);
                        for(k=20;k>=0;k--)
                        {
                                r = r0 - k*(s/20);
                                bot = r / sqrt(4*alfa*t);
                                Ts = T0 - A * myIntegral(bot, top);
                                cout<<r*1000<<"\t"<<Ts<<endl;
                        }

                }
                break;
        }

        //check if the solidification ends
        if(Tm<=Teu){
                //print out the ending temperature
                cout<<"\n Solidification stoped.\n";
                cout<<endl<<t<<"\t"<<s<<"\t"<<T0<<"\t"<<Tm<<"\t"<<deltaT;

                return 0;
        }

        if(deltaT < 0)
                break;

} //end of calculation after stopping T0

return(0);
}

void getTb()
{
        int i;

        //set the boundary temperature
        T[cur*MAX_GRID + I +1] = Tm;

        //initialize the array of the linear systems
        r = 0;
        rr =0;
        rl =0;

        alfa2 = getAlfa2();

        for(i=1;i<=I;i++)
        {       r += i*deltaR;
                rr = r + deltaR/2;
                rl = r - deltaR/2;
                t0 = T[pre*MAX_GRID + i -1];
                t1 = T[pre*MAX_GRID + i +0];
                t2 = T[pre*MAX_GRID + i +1];
                Tarray[(i)*4+0] = (-1)*(1-theta)*rl;
                Tarray[(i)*4+1] = deltaR*deltaR*r/(alfa2*deltaT) + 2*(1-theta)*r;
                Tarray[(i)*4+2] = (-1)*(1-theta)*rr;
```

```
                    Tarray[(i)*4+3] = theta*rl*t0 + ( deltaR*deltaR*r/(alfa2*deltaT) - 2*theta*r )*t1 +
theta*rr*t2;
            }
            Tarray[1*4 + 1] += Tarray[1*4 + 0];
            Tarray[I*4 + 3] -= Tarray[I*4 +2] * Tm;

            //Gauss eliminition
            double ratio;
            for(i=2;i<=I;i++)
            {
                    ratio = Tarray[i*4+0] / Tarray[(i-1)*4+1];
                    Tarray[i*4+0] = Tarray[i*4+0] - Tarray[(i-1)*4+1]*ratio; // =0
                    Tarray[i*4+1] = Tarray[i*4+1] - Tarray[(i-1)*4+2]*ratio;
                    Tarray[i*4+3] = Tarray[i*4+3] - Tarray[(i-1)*4+3]*ratio;

            }
            Tarray[I*4 + 3] = Tarray[I*4 + 3] / Tarray[I*4 +1];
            Tarray[I*4 + 1] = 1;
            for(i=I-1;i>=1;i--)
            {
                    ratio = Tarray[(i)*4+2];
                    Tarray[i*4+3] -= Tarray[(i+1)*4+3]*ratio;
                    Tarray[i*4+2] = 0;
                    Tarray[i*4+3] = Tarray[i*4+3]/Tarray[i*4+1];
            }


            //store the new value
            for(i=1;i<=I;i++)
            {
                    T[cur*MAX_GRID + i] = Tarray[i*4+3];
            }
            T[cur*MAX_GRID + 0] = T[cur*MAX_GRID + 1];

            Tb = T[cur*MAX_GRID + I];        //the point next to the melting interface
}

double getAlfa2()
{
            double K1, K2, P1, P2, Cp1, Cp2, K0, P0, Cp0;
            double portion;

            //proportion of para-DCB to total melt
            portion = 1 - r0*r0*(1-Xinit)/( (r0-s)*(r0-s) );

            //parameters for para-DCB
            K1 = 0.105;      // W/(m K)
            P1 = 1.2475e6;   // g/m3
            Cp1= 1.188;              // J/gK

            //paramters for ortho-DCB
            K2 = 0.121; // W/(m K)
            P2 = 1.3022e6;   // g/m3
            Cp2= 1.159;              // J/gK

            //the paramters for the melt by proportion
            K0 = portion*K1 + (1-portion)*K2;
```

```
        P0 = portion*K1 + (1-portion)*P2;
        Cp0= portion*Cp1 + (1-portion)*Cp2;

        return K0 / (P0*Cp0);
}

void UpdateKmP(double ss)
{
        double K1, K2, P1, P2, Cp1, Cp2;
        double portion;

        //proportion of para-DCB to total melt
        portion = 1 - r0*r0*(1-Xinit)/( (r0-ss)*(r0-ss) );

        //parameters for para-DCB
        K1 = 0.105;        // W/(m K)
        P1 = 1.2475e6;    // g/m3
        Cp1= 1.188;                // J/g

        //paramters for ortho-DCB
        K2 = 0.121; // W/(m K)
        P2 = 1.3022e6;    // g/m3
        Cp2= 1.159;                // J/g

        //the paramters for the melt by proportion
        Km = portion*K1 + (1-portion)*K2;
        P1 = portion*K1 + (1-portion)*P2;

        return;
}
```

Program 3: Source code for calculation of eutectic temperature

```
/******************************************************************
This program calculates the eutectic temperature for the binary system of the example in
Chapter 5.
******************************************************************/
#include <stdio.h>
#include <math.h>
#include <stdlib.h>

void main()
{
        // 1: ODCB
        // 2: PDCB
        double dHaf1 = 18160;
        double dHaf2 = 12930;
        double R       = 8.32;
        double Taf1     = 326.1;
        double Taf2     = 256;
        double a, b, c, d;
        double Tm1, Tm2, Tm, f1, f2, f;

        double Xliquid1, Xliquid2;

        a = dHaf1/R/Taf1;
        b = dHaf1/R;
        c = dHaf2/R/Taf2;
        d = dHaf2/R;

        Tm1 = 360;
        Tm2 = 100;
        Tm = (Tm1 + Tm2)/2;
        printf("\n%lf\t%lf\t%lf",Tm1,Tm,Tm2);

        do{

                f1 = exp(a - b /Tm1) + exp(c - d/Tm1) - 1;
                f2 = exp(a - b /Tm2) + exp(c - d/Tm2) - 1;
                f  = exp(a - b /Tm ) + exp(c - d/Tm ) - 1;

                if(f1 * f <=0)
                        Tm2 = Tm;
                else if(f2 *f<=0)
                        Tm1 = Tm;
                else{
                        printf("\nerror!");
                        exit(0);
                }


                Tm = (Tm1 + Tm2)/2;
                printf("\n%lf\t%lf\t%lf",Tm1,Tm,Tm2);

        }while(fabs(Tm - Tm2)>0.000001);
```

```
Xliquid1 = exp(dHaf1/R*(1/Taf1 - 1/Tm));
Xliquid2 = exp(dHaf2/R*(1/Taf2 - 1/Tm));

printf("\nFinal: Tm = %lf\tX1 = %lf\tX2 = %lf\n",Tm,Xliquid1,Xliquid2);


}
```

REFERENCES

[1] Philip A. Schweitzer, Handbook of Separation Techniques for Chemical Engineers, McGraw-Hill Professional, 1997.

[2] A.Chianese and N.Santilli (1998), Modeling of the solid layer growth from melt crystallization – the integral formulation approach, Chemical Engineering Science, Vol. 53, No. 1, pp. 107-111.

[3] Ulrich, J., Kuszlik, A., Özouz, Y., Crystallization from the melt - a low energy consuming separation process. Journal of Separation Process Technologies, Vol10 (1989) pp33 – 38.

[4] Wynn, N. P. (1986) Chem. Engng Prog. 82, pp26-27.

[5] Matsuoka, M., in J. Garside, R. J. Davey, and A. G. Jones (eds.), "Advances in Industrial Crystallization," Butterworth-Heinemann, Oxford, UK, 1991. pp. 229-244.

[6] V. J. Beck, B. Blackwell, and C. A. St. Clair, Inverse Heat Conduction, Wiley, New York, 1985.

[7] E. Hensel, Inverse Theory and Applications for Engineers, Prentice Hall, Englewood Cliffs, N.J., 1991.

[8] O.M. Alifanov, An Introduction to the Theory of Inverse of Inverse Heat Transfer Problems, Mashinestroenie Publishing Agency, Moscow, 1991.

[9] O.M.Alifanov, High Temp, 15, 498-504, 1977.

[10] V.J.Beck, Int. J. Heat Mass Transfer 13, 703-716, 1970.

[11] C.F.Weber, Int. J. Heat Mass Transfer 24, 1783-1792, 1981.

[12] A.N.Tikhonov and V.Y.Arsenin, Solutions of Ill-Posed Problems, Winston & Sons, Washington, DC, 1977.

[13] G. Stoltz, Jr., J. Heat Transfer 82, 20-26, 1960.

[14] J. V. Beck, Nucl. Eng. Des. 7, 170-178, 1968.

[15] J. V. Beck, ASME Paper, No. 75-WA/HT, 1982.

[16] J.V.Beck and H. Wolf, ASME Paper, No.65-HT-40, 1965.

[17] O.R.Burggraf, J. Heat Transfer 86, 373-382, 1964.

[18] M. Imber and J. Khan, AIAA Journal 10, 784-789, 1972.

[19] D. Langford, Q. Appl. Math. 24, 315-322, 1967.

[20] C. F. Weber, Int. J. Heat Mass Transfer 24, 173-1792, 1981.

[21] W. B. Powell and T. W. Price, ISA Trans 3, 246-254, 1964.

[22] T. P. Fidelle and G. E. Zinsmeister, ASME Paper, No. 68-WA/HT-26, 1968.

[23] J.V.Beck, Int. J. Heat Mass Transfer 13, 703-716, 1970.

[24] N. D'Souza, ASME Paper, No.75-WA/HT-81, 1975.

[25] L. Garifo, V. E. Schrock, and E. Spedicato, Energia Nucleare 22, 452-464, 1975.

[26] J. D. Randal, Technical Report, John Hopkins University, Laural, MD, 1976.

[27] J. V. Beck, B. Litkovhi, and C. R. St. Clair, Num. Heat Transfer 5, 275-286, 1982.

[28] B. F. Blackwell, M., Num. Heat Transfer 4, 229-239, 1981.

[29] B. R. f. Bass and L. J. Ott, Adv. Comp. Tech. 2, 238-248, 1980.

[30] P. S. Hore, G. W. Krutz, and R. J. Schoenhals, ASME Paper, No. 77-WA/TM-4, 1977.

[31] B. R. f Bass, J. Heat Transfer 85, 378-379, 1963.

[32] W. Bennon and F. Incropera, A Continuum Model for Momentum, Heat and Species Transport in Binary Solid-Liquid Phase Change Systems-I. Model Formulation, Int. J. Heat Mass Transfer, vol. 30, pp. 2161-2170, 1987.

[33] C. Beckermann and R. Viskanta, Double Di.usive Convection during Dendritic Solidification of a Binary Mixture, PhysicoChem Hydrodyn, vol. 10, pp. 195-213, 1988.

[34] A.B. Crowley and J.R. Ockendon, On the Numerical Solution of an Alloy Solidification Problem, Int. J. Heat Mass Transfer, vol. 22, pp. 941-946, 1979.

[35] 5. D.L. Feltham and J. Garside, Analytical and Numerical Solutions Describing the Inward Solidification of a Binary Melt, Chemical Engineering Science, vol. 56, pp. 2357-2370,2001.

[36] R.M. Furzeland, A Comparative Study of Numerical Methods for Moving Boundary Problems, Journal of the Institute of Mathematical Application, vol. 26, pp. 411-429, 1980.

[37] S. Ganesan and D. Poirier, Conservation of Mass and Momentum for the Flow of Finterdendritic Liquid during Solidification, Metallurgical Transactions, vol. B21B, pp. 173-181, 1990.

[38] S.W. Gilbert, Melt Crystallization: Process Analysis and Optimization, AIChE Journal, vol. 37, pp. 1205-1215, 1991.

[39] R. Guardani, S.M.S. Neiro, H. Bulau and J. Ulrich, Experimental Comparison and Simulation of Static and Dynamic Solid Layer Melt Crystallization, Chemical Engineering Science, vol. 56, pp. 2371-2379, 2001.

[40] R. Guardani and A. Belline, Application of Mathematical Modeling in a Two-Component Layer Crystallization Process, Chemical Engineering Technology, vol. 20, pp. 495-501, 1997.

[41] S.C. Gupta, Analytical and Numerical Solutions of Radially Symmetric inward Solidification Problems in Spherical Geometry, Int. J. Heat Mass Transfer, vol. 30, pp. 2611-2616, 1987.

[42] S. Henning and J. Ulrich, Description of the Migration of Liquid Inclusions in Growing Crystalline Layers, Transactions of the IchemE, Part A, vol. 75, pp. 233-236, 1997.

[43] H.E. Huppert, The Fluid Mechanics of Solidification, Journal of Fluid Mechanics, vol. 212. pp. 209-240, 1990.

[44] S. Idelsohn, N. Nigro, and M. Storti, Segregation in Continuous Casting Processes with Coupled Solidification and Fluid Flow Modeling, Int. J. Forming Process, vol. 1, pp. 135-162, 1998.

[45] J.S. Langer, Instabilities and Pattern Formation in Crystal Growth, Reviews of Modern Physics, vol. 52, pp.1-28, 1980.

[46] W.W. Mullins and R.F Sekerka, Stability of a Planar Interface during Solidification of a Dilute Binary Alloy, Journal of Applied Physics, vol.35, pp. 444-451, 1964.

[47] N. Nigrop, A. Uespe, and V. Fachinotti, Phasewise Numerical Integration of Finite Element Method Applied to Solidification Processes, Internal Journal of Heat and Mass Transfer, vol. 5, pp. 1053-1066, 2000.

[48] R.I. Pedroso and G.A. Domoto, Inward Spherical Solidification-Solution by the Method of Strained Coordinates, Int. J. Heat Mass Transfer, vol.16, pp.1037-1043, 1973.

[49] G. Poots, On the Application of Integral-Methods to the Solution of Problems Involving the Solidification of Liquids Initially at Fusion Temperature, Int. J. Heat Mass Transfer, vol. 5, pp. 525-531, 1962.

[50] P. Prescott, F. Incropera, and W. Bennon, Modeling of Dendritic Solidification Systems: Reassessment of the Continuum Momentum Equation, Int. J. Heat Mass Transfer, vol.34, pp. 2351-2359, 1991.

[51] D.S. Riley, F.T Smith and G. Poots, The Inward Solidification of Spheres and Circular Cylinders, Int. J. Heat Mass Transfer, vol.17, pp.1507-1516, 1974.

[52] M. Salcudean, Z. Abdullah, On the Numerical Modeling of Heat Transfer during Solidification Processes, Int. J. Heat Mass Transfer, vol. 25, pp. 445-473, 1988.

[53] R. Scholz, K. Wangnik and J. Ulrich, On the Distribution and Movement of Impurities in Crystalline Layers in Melt Crystallization Processes, Journal of Physics D, vol. 26, pp. B156-B161, 1993.

[54] Y.P. Shih and S.Y. Tsay, Analytical Solutions for Freezing a Saturated Liquid Insider or Outside Cylinders, Chemical Engineering Science, vol. 26, pp. 809-816, 1971.

[55] D.W. Slaughter and M.F. Doherty, Calculation of Solid-Liquid Equilibrium and Crystallization Paths for Melt Crystallization Processes, Chemical Engineering Science, vol.50, pp. 1679-1694, 1995.

[56] A.M. Soward, A Unified Approach to Stefan's Problem for Spheres and Cylinders, Proceedings of the Royal Society, London Series A, vol. 373, pp.131-147, 1980.

[57] K. Stewartson and R.T. Waechter, On Stefan's Problem for Spheres, Proceedings of the Royal Society, London Series A, vol. 348 pp. 415-426, 1976.

[58] L.C. Tao, Generalized Numerical Solution of Freezing a Saturated Liquid in Cylinders and Spheres, AIChE Journal, vol.13, pp. 481-501,1967.

[59] V. Voller and C. Prakash, A Fixed Grid Numerical Modeling Methodology for Convection-Di.usion Mushy Region Phase Change Problems, Int. J. Heat Mass Transfer, vol. 30, pp.1709-1719, 1987.

[60] V. Voller, A. Brent and C. Prakash, The Modeling of Heat, Mass and Solute Transport in Solidification Systems, Applied Math. Modeling, vol.14, pp. 320-326, 1990.

[61] K. Wangnick and J. Ulrich, A Model for the Calculation of the Purification E.ciency of a Solid Layer Melt Crystallization Process, Crystal Research and Technology, vol. 29, pp. 349-356, 1994.

[62] W. Dai, Z. Feng, R. Nassar and J. Palmer, A combined analytic and numerical method for predicting the solid layer growth from melt crystallization, Numerical Heat Transfer, Part A, vol. 44, pp. 577-590, 2003.

[63] Arkenbout, G. F. Melt crystallization technology. Lancaster Technomic Publishing. 1995.

[64] Sloan, G. J., and McGhie, A. R., "Techniques of Melt Crystallization", John Wiley and Sons, New York, 1988.

[65] R. Haase, Thermodynamik der Mischphasen, Springer, New Youk,1956.

[66] S.M. Walas, Phase Equilibria in Chemical Engineering, Butterwoth-Heinemann, UK,1985.

[67] J.M. Dowden, The Mathematics of Thermal Modeling, Chapman & Hall/CRC, New York, Chaps. 4 and 5, 2001.

[68] R.L. Burden and J.D. Faires, Numerical Analysis, sixth edition, Brooks/Cole, 1997.

[69] S. B. Gaikwad, B.N.Thorat and S. B. Sawant, Separation Technology: Melt Crystallization, Chemical Weekly, 48(14), 187-191, 2002

[70] SRI Chemical and Economics Handbook, "Chlorobenzene Production," Menlo Park, CA, 1989.

[71] Locating and Estimating Air Emissions from Sources of Chlorobenzenes (revised), Office of Air Quality Planning and Standards, U.S. Environmental Protection Agency, March 1994.

[72] http://www.goodwill-india.com/prod1.htm

[73] Priority Existing Chemical Assessment Report No. 13, National Industrial Chemicals Notification and Assessment Scheme (NICNAS), 2000.

[74] Priority Existing Chemical Assessment Report No. 14, National Industrial Chemicals Notification and Assessment Scheme (NICNAS), 2001.

[75] P.J. Linstrom and W.G. Mallard, NIST Chemistry WebBook, NIST Standard Reference Database, Number 69, July 2001 (http://webbook.nist.gov/chemistry).

[76] Sulzer Chemtech Ltd, http://www.sulzerchemtech.com/

[77] BEFS Technologies, http://www.befs.com

[78] Guardani, R.; Neiro, S. M.; Bulau, H.; Ulrich, J., Experimental comparison and simulation of static and dynamic solid layer melt crystallization, Chemical Engineering Science, 2001, vol. 56, no. ER7, pp. 2371-2379.

[79] E. L. Anderson, Chemical Industry, 131-136, 1975.

[80] J. C. Brice and P. A. C. Whiffin, Solid State Electronics, 7, 183, 1964.

[81] H. Schildknecht, Zone Melting, Academic, New York, 1966, pp. 113-117.

[82] J. C. Maire and M. A. Delmas, Rec. Trav. Chim. Pays Bas, 85, 268-274, 1966.

[83] A. R, McGhie, P. J. Rennolds, and G. J. Sloan, Anal. Chem., 52, 1738-1742, 1980.

[84] G. H. Moates and J. K. Kennedy, Continuous Zone Melting, Fractional Solidification, Vol 1, Dekker, New York, 1967.

[85] E. F. G. Herington and I. J. Lawrenson, J. Appl. Chem., 19, 341-344, 1969.

[86] E. F. G. Herington and I. J. Lawrenson, Nature, 219, 928, 1968.

[87] E. F. G. Herington and I. J. Lawrenson, J. Appl. Chem., 19, 337-341, 1969.

[88] F. N. Rhines, Phase Diagrams in Metallurgy, McGraw-Hill, New York, 1956, p. 25.

[89] F. N. Rhines, An Overview of the Determination of Phase Diagrams, in Applications of PhaseDiagrams in Metallurgy and Ceramics, Proceedings of a Workshop at National Bureau of Standards, Gaithersburg, MD, Jan. 1977, NBS-SP496.